

CERN-TH/98-28

SHEP-98/05

hep-ph/9804283

Lepton Flavour Violation in String-Inspired Models

S. F. King^{† 1} and M.Oliveira^{* 2}

[†] *Theory Division, CERN, CH-1211 Geneva 23, Switzerland*

^{*} *Department of Physics and Astronomy, University of Southampton
Southampton, SO17 1BJ, U.K*

Abstract

Lepton flavour violation (LFV) has been proposed as a significant test of supersymmetric unification. Here we show that such signals are also a generic feature of supersymmetric string unified models in which there is no simple unified gauge group. In realistic models of this kind which involve third family Yukawa unification and large values of $\tan\beta$, there are generally heavy right-handed (singlet) neutrinos of intermediate mass M_ν , whose couplings violate lepton flavour. To illustrate these effects we calculate the rates for $\mu \rightarrow e + \gamma$ and $\tau \rightarrow \mu + \gamma$ in the minimal supersymmetric $SU(4) \otimes SU(2)_L \otimes SU(2)_R$ model. Including only the minimum irreducible contributions, we find that both rates are enhanced relative to similar models with low $\tan\beta$, with $\tau \rightarrow \mu + \gamma$ providing a decisive test of such models in the near future.

CERN-TH/98-28

January 29, 2018

¹On leave of absence from *.

²Work supported by JNICT under contract grant : PRAXIS XXI/BD/5536/95.

1 Introduction.

Recently there has been much interest in lepton flavour violation (LFV) as a probe of physics beyond the standard model triggered by the observation of Barbieri and Hall [1, 2] that processes such as $\mu \rightarrow e + \gamma$ might be very good low energy signals of supersymmetric grand unified theories (SUSY GUTs). In the standard model separate lepton numbers L_e, L_μ, L_τ are exactly conserved, which explains the absence of LFV to remarkable accuracy (the present limit on the branching ratio for $\mu \rightarrow e + \gamma$ is approaching 10^{-11} .) Even if small neutrino masses are introduced into the standard model, thereby violating separate lepton numbers, the effect on $\mu \rightarrow e + \gamma$ is very small, since the amplitude is proportional to $\Delta m_\nu^2/M_W^4$ multiplied by suitable mixing angles, where Δm_ν^2 is the difference in the squared masses of two neutrino species, and M_W is the W boson mass. The introduction of SUSY allows the possibility of larger contributions to such processes since the soft SUSY breaking masses and couplings may violate separate lepton numbers by arbitrarily large amounts. This means that in SUSY there are in general additional diagrams which have in principle large contributions to LFV processes [3].

One way to avoid conflict with the experimental limits is to invoke some supergravity (SUGRA) theory [4] which leads to universal soft parameters at the Planck scale [5]. In the absence of radiative corrections the selectron mass matrix in the basis $\tilde{e}, \tilde{e}^{c*}$ would look like

$$\begin{pmatrix} m_e^\dagger m_e + m_{3/2}^2 I & A m_e \\ A^* m_e^\dagger & m_e m_e^\dagger + m_{3/2}^2 I \end{pmatrix} \quad (1)$$

where m_e is the electron mass matrix, I is the unit matrix, and $m_{3/2}, A$ are universal soft parameters. Clearly each 3×3 block of the selectron mass matrix becomes diagonal in the basis in which the electron mass matrix is diagonal, which implies no LFV. Any violation of universality will lead to off-diagonal elements in the 3×3 blocks of the slepton matrix in the charged lepton mass basis, which implies LFV. In

the minimal supersymmetric standard model (MSSM) this result is preserved even in the presence of radiative corrections. This is because the renormalisation group (RG) equations do not generate any off-diagonal elements for squark masses in a basis in which the charged lepton Yukawa couplings are diagonal. Clearly if the universality assumption is relaxed then arbitrarily large LFV is possible in the MSSM. The observation of Barbieri and Hall is that with SUSY GUTs LFV is unavoidable, even with the assumption of universality. Part of the reason is that in GUTs, quarks and leptons share a common multiplet so that the lepton sector is contaminated by the flavour violating quarks. Without SUSY such an effect, though present, would be generally very weak as it scales with an inverse power of the scale of the unification scale M_{GUT} . However in the presence of SUSY the RG running of the slepton masses between M_P and M_{GUT} causes the LFV to be imprinted onto the slepton masses, which are no longer diagonal in the basis in which the leptons are diagonal. Below the GUT scale the MSSM RGEs then ensure that the LFV effect is preserved down to the TeV scale where it may lead to sizeable contributions to physical processes.

Although LFV can be interpreted as a signal of SUSY GUTs such as $SU(5)$, $SO(10)$ [1, 2] similar effects can be achieved without the presence of a GUT gauge group, even assuming strictly universal soft parameters at M_P . For example, simply adding a right-handed neutrino to the MSSM (MSSM+ ν) [6] will generate LFV effects due to the fact neutrino that (Dirac) Yukawa couplings are not diagonal in the basis in which the charged lepton Yukawa couplings are diagonal. In the charged lepton mass basis the non-diagonal neutrino Yukawa matrix will generate off-diagonal slepton masses due to the RG running of the slepton mass matrix between M_P and the scale M_ν , where M_ν is the Majorana mass scale of the right-handed neutrinos. This will result in low energy LFV effects rather similar to those in SUSY GUTs, but without any underlying GUT gauge group. However the MSSM+ ν theory is rather unconstrained compared to SUSY GUTs, and it is of interest to see if similar effects

could occur in other better motivated, but non-GUT models. In particular we have in mind string-inspired models which do not involve a simple gauge group, but where the gauge couplings are unified at the string scale.

In this paper we shall focus on a particular recently proposed string-inspired model, the minimal supersymmetric $SU(4) \otimes SU(2)_L \otimes SU(2)_R$ model [7] (see also [8, 9]). In this model, quarks and leptons are unified into common multiplets, but there is no simple GUT gauge group. Instead the gauge couplings are unified with gravity at the string scale. In the minimal version [7] the only source of LFV in the 422 model is via the right-handed neutrino couplings, as in the MSSM+ ν model. However, unlike the MSSM+ ν model, the minimal 422 model is much more highly constrained. For example in minimal 422 there is complete Yukawa unification for the third family top, bottom, tau and tau-neutrino Yukawa couplings, which automatically leads to the prediction of a large ratio of Higgs vacuum expectation values (VEVs) with $\tan\beta$ in the range 30-60 [10] which lies beyond the scope of the results presented in [6]. As discussed in [11] the large $\tan\beta$ region involves some new effects which were neglected in previous treatments, and we are careful to include all relevant effects here.

It is worth comparing the minimal string inspired $SU(4) \otimes SU(2)_L \otimes SU(2)_R$ model to $SO(10)$, which also may have Yukawa unification. In $SO(10)$ colour triplets with couplings to fermions are inevitably present in the effective theory beneath M_P . Indeed in $SU(5)$ this is the primary source of LFV. But in minimal 422 such colour triplets, although generically present, do not couple to fermions, and play no role in LFV.³ In general it is easy to introduce new sources of LFV, for example via LFV soft mass terms which for example may be controlled by additional $U(1)_X$ gauged family symmetries [12]. Our approach here is to consider the *minimum irreducible* amount

³ In a non-minimal 422 model this source of flavour violation could be included at the cost of introducing eighteen unconstrained new parameters.

of LFV associated with this class of model. Such an approach allows unavoidable constraints to be placed on the model from the experimental limits on LFV.

Concerning our results, we find that the diagrams involving sneutrinos and charginos in the loop are found to give the dominant contribution to $\mu \rightarrow e + \gamma$ and $\tau \rightarrow \mu + \gamma$. The off-diagonal sneutrino masses, which are responsible for LFV, receive contributions from two distinct sources: F-term Dirac neutrino masses (which always occur at the electroweak scale despite the fact that the right-handed neutrinos are much heavier) and RGE evolution in the high energy region between the Planck scale and the right-handed neutrino mass scale. Although both effects result from the neutrino Yukawa couplings, they enter with opposite sign, and can lead to cancellations in some regions of parameter space. Nevertheless in the minimal supersymmetric $SU(4) \otimes SU(2)_L \otimes SU(2)_R$ model, with realistic masses and mixing angles, we find that generally that the rates are enhanced relative to the low $\tan\beta$ case due to increased 12 and 23 family mixing effects. In particular we find that the predicted rate for $\tau \rightarrow \mu + \gamma$ is quite close to the current experimental limit.

The organisation of the rest of the paper is as follows. In Section 2 we review the minimal 422 model. In Section 3 we describe in detail how the model was implemented giving particular emphasis to boundary conditions of the RGEs. Section 4 is devoted to a detailed analysis of the one-loop decay $\mu \rightarrow e + \gamma$ and $\tau \rightarrow \mu + \gamma$. Section 5 contains our conclusions.

2 The Model.

Above M_{PS} we have adopted a model with unified gauge group [8]

$$G_{PS} = SU(4) \otimes SU(2)_L \otimes SU(2)_R \quad (2)$$

Here we briefly summarise the parts that are relevant for our analysis. For a more complete discussion see [9]. The left-handed quarks and leptons are accommodated

in the following $F = (4, 2, 1)$, $F^c = (\bar{4}, 1, \bar{2})$ representations :

$$F_i = \begin{pmatrix} u^r & u^b & u^g & \nu \\ d^r & d^b & d^g & e \end{pmatrix}_i \quad F_j^c = \begin{pmatrix} d_r^c & d_b^c & d_g^c & e^c \\ u_r^c & u_b^c & u_g^c & \nu^c \end{pmatrix}_j \quad (3)$$

where $i, j = 1 \dots 3$ is a family index. The MSSM Higgs fields are contained in $h = (1, \bar{2}, 2)$:

$$h = \begin{pmatrix} H_u^0 & H_d^+ \\ H_u^- & H_d^0 \end{pmatrix} \quad (4)$$

whereas the heavy Higgs $H = (4, 1, 2)$ and $H^c = (\bar{4}, 1, \bar{2})$ are denoted:

$$H = \begin{pmatrix} H_{ur} & H_{ub} & H_{ug} & H_\nu \\ H_{dr} & H_{db} & H_{dg} & H_e \end{pmatrix} \quad H^c = \begin{pmatrix} H_{ur}^c & H_{ub}^c & H_{ug}^c & H_{\nu^c} \\ H_{dr}^c & H_{db}^c & H_{dg}^c & H_{e^c} \end{pmatrix} \quad (5)$$

In addition to the Higgs fields in (4) and (5) the model also involves an $SU(4)$ sextet field $D = (6, 1, 1) = (D_3, D_3^c)$.

The superpotential of the minimal 422 model is [7]:

$$\begin{aligned} \mathcal{W} = & S[\kappa(H^c H - M_{PS}^2) + \lambda h^2] + \lambda_H D H H + \lambda_{H^c} D H^c H^c \\ & + \lambda_{33} F^c{}_3 F_3 h + \lambda_{ij} F^c{}_i F_j h \frac{(H^c H)^n}{M_P^{2n}} + \lambda_{\nu ij} \frac{F^c{}_i F_j H H}{M_P} \end{aligned} \quad (6)$$

where S denotes a gauge singlet superfield, the parameters κ, λ and M_{PS} are taken to be real and positive, and h^2 denotes the unique bilinear invariant $\epsilon^{ij} h_i^{(1)} h_j^{(2)}$. Also, $M_P (\simeq 2.4 \times 10^{18} \text{ GeV})$ denotes the ‘reduced’ Planck mass. As a result of the superpotential terms involving the singlet S the Higgs fields develop VEVs, $\langle H \rangle = \langle H_\nu \rangle \sim M_{PS}$ and $\langle H^c \rangle = \langle H_{\nu^c} \rangle \sim M_{PS}$, which lead to symmetry breaking

$$SU(4) \otimes SU(2)_L \otimes SU(2)_R \rightarrow SU(3)_c \otimes SU(2)_L \otimes U(1)_Y. \quad (7)$$

The singlet S itself also naturally develops a small VEV of order the SUSY breaking scale [7] so that the λS term in (6) gives an effective μ parameter of the correct order of magnitude. Under (7) the Higgs field h in (4) splits into the familiar MSSM doublets H_u and H_d whose neutral components subsequently develop weak scale VEVs $H_u^0 = \langle v_u \rangle$ and $H_d^0 = \langle v_d \rangle$ with $\tan \beta = v_u / v_d$.

This model has Yukawa unification for the third family [13, 14] which leads to a large top mass $m_{top} > 165$ GeV and $\tan\beta \sim m_{top}/m_{bottom}$. First and second family Yukawa couplings are effectively generated by non-renormalisable operators which are suppressed by powers of a heavy scale $M > M_{GUT}$. In the 422 model, these operators can be constructed from different theoretical group contractions of the fields such as [15]:

$$\mathcal{O}_{ij} = F_i^c \lambda_{ij} F_j h \left(\frac{H H^c}{M_P^2} \right) + \text{h.c.} \quad (8)$$

The idea is that when the heavy Higgs develop their large VEVs such operators reduce to effective Yukawa couplings of the form $F^c \lambda F$ with a small (M_{PS}^2/M_P^2) coefficient. Assuming a (well motivated) texture [17] for the Yukawa matrix at M_{PS} and suitably choosing a set of operators, successful predictions can be made for some SM parameters. Vertical splittings within a particular family are accounted for by group theoretical Clebsch factors [15]. A detailed analysis of this approach for the 422 model can be found in [18]. The non-renormalisable operators involving the right-handed neutrino result in Majorana masses of the form $1/2 M_\nu \nu^c \nu^c$, where $M_\nu \sim M_{PS}^2/M_P$, which enables right-handed neutrinos to decouple at the scale M_ν , leading to a Gell-Mann-Ramond-Slansky see-saw mechanism.

The D field doesn't develop a VEV but the terms HHD and $H^c H^c D$ combine the colour triplets parts of H , H^c and D into acceptable GUT scale mass terms [9]. We note that the 422 symmetry also allows the couplings :

$$FFD \rightarrow QQD_3 + QLD_3^c \quad (9)$$

$$F^c F^c D \rightarrow u^c d^c D_3^c + u^c e^c D_3 + d^c \nu^c D_3 \quad (10)$$

which obviously would generate additional LFV signals. However these may be forbidden by a global R-symmetry [7]. Their exclusion here is in keeping with the general philosophy of the approach which is to consider the minimum amount of irremovable LFV in the model, so that LFV becomes an unavoidable signal of the model.

3 Procedure.

In this section we describe how the 422 model was implemented. We considered three fundamental scales : M_{SUSY} which was assumed to equal the top mass, $M_{GUT} \sim 2 \times 10^{16}$ GeV the scale of coupling unification and $M_{Planck} \sim 2 \times 10^{18}$ GeV. An additional scale M_ν describing the energy at which the right-handed neutrinos decouple via see-saw mechanism was introduced. Cosmological constraints require 10^{10} GeV $\leq M_\nu \leq M_{GUT}$ [19]. Experimentally viable boundary conditions were imposed at each fundamental scale and we used one-loop matrix RGEs [20] to relate parameters at different energies (particle threshold effects were ignored).

We now turn to describe the algorithm of the program. Since we want to achieve third family Yukawa unification (3FYU) at M_{GUT} [21], which crucially depends on the unknown low energy values of m_{top} , $m_{\nu_\tau} = v_u \lambda_{\nu_\tau}$ and $\tan \beta$ a iterative procedure is needed. Initial estimates for these parameters are guessed and, along with gauge couplings and all Yukawa matrices, are run, first from their definition values to $M_{SUSY} = m_{top}$ and afterwards from M_{SUSY} to M_{GUT} . At M_{GUT} the guesses are tested to see if they actually lead to 3FYU. This is unlikely to happen in the first attempt therefore we induce slight changes in our initial guesses and repeat the above process again. After a few iterations it starts to be obvious that some guesses are more successful than others. These are subjected to further perturbative analysis allowing more precise GUT unification. This recursive approach is repeated many times until the condition $\lambda_t = \lambda_b = \lambda_{\nu_\tau} = \lambda_\tau$ is verified to a satisfactory accuracy (typically 1%). At this point some comments are worth making. The running of masses to M_{SUSY} was done using Standard Model RGE (one-loop QED, three-loop QCD [22]) and it is necessary as it provides important mass corrections especially for light quarks. After the whole iterative process is complete we are left with predictions for our guesses based on the assumption of 3FYU. To have an idea, for the input $\alpha_s = 0.115$, $m_b = 4.25$

GeV, $M_\nu = M_{GUT}$ we obtained the following values $m_{top} \sim 175$ GeV, $m_{\nu_\tau} \sim 122$ GeV and $\tan \beta \sim 56$. The dependence on M_ν is mostly felt by m_{ν_τ} which can decrease to 115 GeV when $M_\nu \sim 10^{12}$ GeV. The variations with α_s and m_b are considerable and well documented [18]. We note that it is important to watch for the magnitude of the third family of the Yukawa couplings at M_{Planck} because they are very sensitive to α_s and M_ν , therefore can easily acquire values outside the range allowed in perturbative regime (Figure 1).

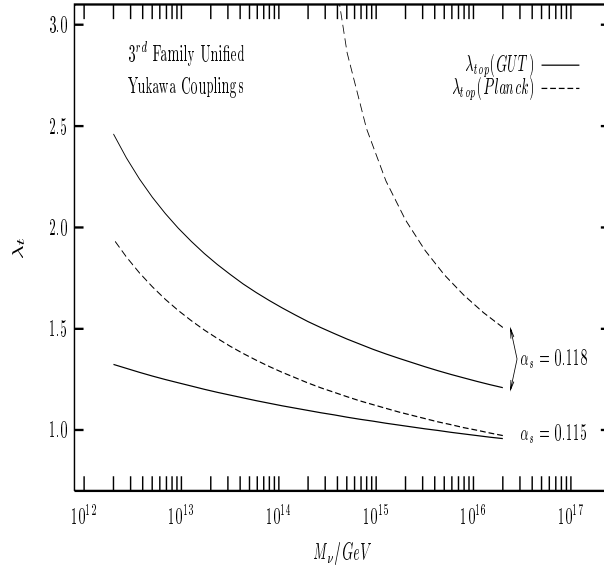


Figure 1. Dependence of third family unified Yukawa coupling λ_{top} at GUT (solid) and Planck (dashed) energy with the right-handed neutrino decoupling scale M_ν for two values of α_s .

At M_{PS} , we must match all the Yukawa matrix couplings to the ones which can be obtained from non-renormalized operators like Eq.(8). These new Yukawa matrices are not unique. However they are constrained by the fact that they must predict the same (known) physics as the ones they replace, i.e. both must have identical eigenvalues and quark mixing angles (for the sake of simplicity we did not considered CP violating phase). Several forms of these Yukawa matrices were extensively studied in [18, 10] for the 422 model. Here we will only consider the following particular one ⁴ :

⁴Other choices would lead to same order of magnitude results.

$$\lambda_u = \begin{pmatrix} 0 & Y^{n=3} & 0 \\ Y^{Ad} & Y^D - Y^C & 0 \\ 0 & Y^B & Y^{33} \end{pmatrix} \quad (11)$$

$$\lambda_d = \begin{pmatrix} 0 & Y^1 & 0 \\ 3 Y^{Ad} & -(Y^D + Y^C) & 0 \\ 0 & -Y^B & Y^{33} \end{pmatrix} \quad (12)$$

$$\lambda_e = \begin{pmatrix} 0 & Y^1 & 0 \\ 9/4 Y^{Ad} & 3(Y^D + Y^C) & 0 \\ 0 & -Y^B & Y^{33} \end{pmatrix} \quad (13)$$

$$\lambda_\nu = \begin{pmatrix} 0 & Y^{n=3} & 0 \\ 3/4 Y^{Ad} & -3(Y^D - Y^C) & 0 \\ 0 & Y^B & Y^{33} \end{pmatrix} \quad (14)$$

We briefly explain their form. The zeros in positions 31, 13 are motivated by correspondingly small entries on quark CKM matrix. The zero in 23 only effects the right-handed mixing matrix (because of high family hierarchy), thus it is convenient as it improves predictability. Two operators were needed in the 22 position because of particular high charm-muon splitting [18]. The operator Y^B generates $V_{23} \sim V_{32}$, while Y^{Ad} and Y^1 generate $V_{12} \sim V_{21}$ and first family masses.⁵ The coefficients on different matrices associated with the same operator Y are the Clebsh 422 factors mentioned in Section 2. Solutions for Y s were numerically searched for the input: V_{23} , m_{charm} , m_μ and V_{12} , m_{up} , m_e , which enabled three quantities to be predicted : V_{13} , m_{down} , $m_{strange}$ (see Appendix 4 for results). Notice that this model predicts the experimentally unavailable Dirac neutrino masses $m_{\nu_e}, m_{\nu_\mu}, m_{\nu_\tau}$ and the lepton Dirac CKM matrix V^L . The prediction of physical neutrino masses and mixing angles relies on knowledge of the right-handed neutrino Majorana mass matrix M_ν . Following [10] we shall assume that M_ν is proportional to the unit matrix. This rather *ad hoc* assumption at least has the virtue that it leads the result that the modulus of the

⁵Actually, since the $(n=2) Y^1$ operator has a vanishing Clebsh for the up-type fermions, we are forced to introduce a further $Y^{n=3}$ operator in the 12 position, if we want to avoid a massless up quark.

leptonic CKM matrix elements are equal to those calculated just from the Dirac neutrino mass parts [10]. It also means that the physical neutrino masses are determined by a single mass parameter which we continue to denote by M_ν , where this parameter henceforth refers to the overall factor multiplying the unit Majorana matrix rather than the matrix itself. With a suitable choice of M_ν this simple assumption leads to a physical muon-neutrino and electron-neutrino mass spectrum suitable for the MSW solution to the solar neutrino problem, with a tau-neutrino in the correct range for hot dark matter, and with muon-tau neutrino oscillations in the observable range of the CHORUS experiment [10]. If this assumption is relaxed one would generally expect qualitatively similar effects both in the neutrino spectrum, and in the physics of LFV considered here.

After having set experimentally viable Yukawa matrices at M_{PS} , according to the above boundary conditions, we used 422 RGEs (see Appendix 2) to run them to M_P . In this high energy region we treated the theory described in Section 2 in the following effective way. To begin with we regarded the non-renormalisable operators as yielding four effective Yukawa matrices, whose RG evolution is described by standard RGEs appropriate to the larger gauge group $SU(4) \otimes SU(2)_L \otimes SU(2)_R$. The terms involving the singlet S which give rise to an effective μ parameter below the scale M_{PS} , were regarded as an effective μ parameter above this scale similar to the MSSM. Finally we allowed extra D and other superfields to be present above the scale M_{PS} in order to keep the one-loop beta functions of the $SU(4) \otimes SU(2)_L \otimes SU(2)_R$ gauge group equal above this scale, and so allow string gauge unification at M_P [15]. Since such additional superfields do not couple to the quark and lepton superfields their presence will have no effect on the LFV predictions at the one-loop level, apart from the indirect effect via the gauge couplings.

At M_P boundary conditions were chosen to reduce the most the number of independent parameters : $M_i = M_{1/2}$ (common gaugino masses), $\tilde{m}_i^2 = m_{H_{u,d}}^2 = m_0^2$

(universal soft masses), $\tilde{\lambda}_i = A\lambda_i$ (proportional soft Yukawa matrices). With this choice we kept sources of LFV (mass splittings and CKM entries) at a minimum. A departure from the latter two conditions would introduce right from the start LFV signals therefore the results can be interpreted as the irreducible minimum amount of LFV arising from this model.

The next obvious step was to run all the above parameters again down to M_{SUSY} , dropping terms from the RGEs involving right-handed neutrinos and sneutrinos below M_ν . At the low energy SUSY scale we were finally able to set the superpotential Higgs parameter μ^2 and soft Higgs mass $\tilde{\mu}^2$. These were the last parameters to be defined because they obey the following two conditions :

$$\mu^2 = \frac{m_{H_d}^2 - m_{H_u}^2 \tan^2 \beta}{\tan^2 \beta - 1} - 1/2 m_Z^2 \quad (15)$$

$$\tilde{\mu}^2 = 1/2 (m_{H_u}^2 + m_{H_d}^2 + 2\mu^2) \sin 2\beta \quad (16)$$

which depend on the low energy values of $m_{H_u}^2$ and $m_{H_d}^2$ until now unknown. The above equations simply describe how the Higgs VEVs are related to the (classical) renormalised Higgs potential parameters. To see how they came about we recall that after $SU(2) \otimes U(1)_Y \rightarrow U(1)_{QED}$ symmetry breaking the neutral Higgs H_u^0, H_d^0 acquire VEVs v_u, v_d therefore the Higgs potential becomes :

$$\mathcal{V}(H_u, H_d) \rightarrow \mathcal{V}(v_u, v_d) + (\text{Physical Higgs Interactions}) \quad (17)$$

$$\mathcal{V}(v_u, v_d) = (\mu^2 + m_{H_u}^2) v_u^2 + (\mu^2 + m_{H_d}^2) v_d^2 - 2\tilde{\mu}^2 v_u v_d + 1/8 (g'^2 + g^2)(v_u^2 - v_d^2)^2 \quad (18)$$

In order to recover the traditional interpretation of the VEVs, they must satisfy :

$$\frac{\partial \mathcal{V}(v_u, v_d)}{\partial v_u} = 0 \quad \frac{\partial \mathcal{V}(v_u, v_d)}{\partial v_d} = 0 \quad (19)$$

Which after simple algebraic manipulation leads to (15,16), except for obvious replacement of v_u, v_d by the more convenient set $\tan \beta, m_Z$. From (15) we see that μ is determined up to a sign, however we found that for large $\tan \beta$ this arbitrariness was not relevant.

The physical origin of LFV in this model is now clear. The Yukawa coupling matrices are effectively split into λ_u , λ_d , λ_e , λ_ν . These matrices are not equal but related to each other by different Clebsh factors. Since $\lambda_e \neq \lambda_\nu$ one is introducing a CKM like mixing matrix on the lepton sector which gets imprinted onto the left-handed slepton masses due to the RG running between M_P and M_ν (below the scale M_ν the terms involving the right-handed neutrinos are dropped from the RGEs). It is clear that, for example in a basis in which the charged lepton matrix λ_e is diagonal the neutrino matrix λ_ν will be non-diagonal, leading to off diagonal contributions to the left-handed slepton masses of the form ⁶

$$\Delta \tilde{m}_L^2 \sim -\frac{\ln(M_P/M_\nu)}{16\pi^2} m_0^2 (\lambda_\nu^\dagger \lambda_\nu) + \dots \quad (20)$$

It is interesting to note that in $SU(5)$ LFV develops differently. In this model, there is no right-handed neutrino, however, LFV does arise from the presence of Higgs colour triplets which mediate tree level leptoquark interactions, which again leads to off-diagonal slepton masses due to RG running between M_P and M_{GUT} . $SO(10)$ is an example in which both the mentioned LFV processes are active [23, 11].

4 The Processes $\mu \rightarrow e + \gamma$ and $\tau \rightarrow \mu + \gamma$.

4.1 Formalism.

The effective Lagrangian and branch ratio for the decay $\mu \rightarrow e + \gamma$ are given by :

$$\mathcal{L} = 1/2 \bar{u}_e(p-q) \{A_R P_R + A_L P_L\} \sigma^{\alpha\beta} u_\mu(p) \mathcal{F}_{\alpha\beta} \quad (21)$$

$$\text{BR}(\mu \rightarrow e + \gamma) = \frac{12\pi^2}{G_F^2 m_\mu^2} (|A_R|^2 + |A_L|^2) \quad (22)$$

In their most general form, the one-loop amplitudes $A_R = \sum A_{R_i}$, $A_L = \sum A_{L_i}$ are given by a sum of many terms [6] most of which of negligible importance. For sake

⁶There is also an F-term contribution of opposite sign as discussed in Appendix 5.

of simplicity we consider only the dominant contributions :

$$A_{R_1} = \frac{e}{16\pi^2} \frac{x}{\sqrt{2}} (\tilde{U}_{LL}^{n\dagger})_{eA} (\tilde{U}_{LL}^n)_{A\mu} J_{21A} \quad (23)$$

$$A_{R_2} = -\frac{e}{16\pi^2} \frac{x}{2} (\tilde{U}_{LL}^{l\dagger})_{eA} (\tilde{U}_{LL}^l)_{A\mu} (H_{32A} + H_{31A}) \quad (24)$$

$$A_{R_3} = -\frac{e}{16\pi^2} \{ (\tilde{U}_{LL}^{l\dagger})_{eA} (\tilde{U}_{LR}^l)_{A\mu} H_{11A} + (\tilde{U}_{RL}^{l\dagger})_{eA} (\tilde{U}_{RR}^l)_{A\mu} H_{11\dot{A}} \} \quad (25)$$

$$A_{L_1} = \frac{e}{16\pi^2} x (\tilde{U}_{RR}^{l\dagger})_{eA} (\tilde{U}_{RR}^l)_{A\mu} H_{31\dot{A}} \quad (26)$$

$$A_{L_2} = -\frac{e}{16\pi^2} \{ (\tilde{U}_{LR}^{l\dagger})_{eA} (\tilde{U}_{LL}^l)_{A\mu} H_{11A} + (\tilde{U}_{RR}^{l\dagger})_{eA} (\tilde{U}_{RL}^l)_{A\mu} H_{11\dot{A}} \} \quad (27)$$

here written in a notation, which we now explain. In all expressions summation over the family index $A = 1 \dots 3$ is to be understood ($\dot{A} = A + 3$). The factor $x = m_\mu / (\cos \beta m_W)$ and the matrices \tilde{U} and the other factors occuring in these expressions are defined in Appendix 3.

We now discuss the phenomenology of equations (23)-(27). The amplitude $A_L \ll A_R$ because in the 422 model LFVs associated with $\tilde{m}_{e^c}^2$ are negligible compared with the ones due to \tilde{m}_L^2 . Thus we will keep our attention on A_{R_1} , A_{R_2} and A_{R_3} which are associated with the diagrams in Figure 2.

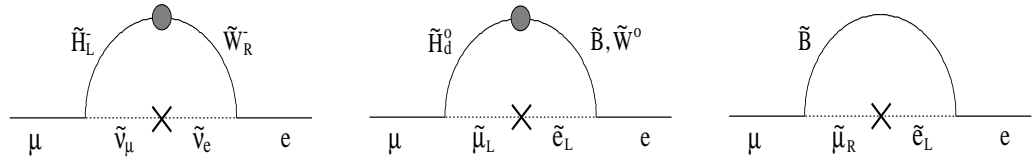


Figure 2. Dominant supersymmetric diagrams involved in the decay $\mu \rightarrow e + \gamma$.

In these, a cross over slepton (dotted) line is introduced to remind us of a $\tilde{U} \tilde{U}$ product dependence. Similarly, the blob over chargino- A_{R_1} (neutralino- $A_{R_{2,3}}$) line stands for $S^C T^C$ ($S^N S^N$) dependence. We stress that, though it is tempting to make a straight analogy with the perturbative mass insertion method valid when $\tan \beta$ is small, such comparison must be taken with great care. For example, if $\tan \beta$ is big

A_{R_3} will have not only a $(\tilde{U}_{LL}^{l\dagger})_{e\mu}(\tilde{U}_{LR}^l)_{\mu\mu}$ contribution but $(\tilde{U}_{LL}^{l\dagger})_{ee}(\tilde{U}_{LR}^l)_{e\mu}$ as well. Nevertheless Figure 2 is useful to the extent it identifies which supersymmetric states are directly involved in each diagram.

The neutralino contributions are A_{R_2} which describes LFV arising from left-handed selectrons ($\tilde{U}_{LL}^l = \tilde{S}_{LL}^l T^{e\dagger} \neq 1$) and A_{R_3} which is related with mixing of chirality ($\tilde{U}_{LR}^l = \tilde{S}_{LR}^l S^{e\dagger}$, $\tilde{U}_{RL}^l = \tilde{S}_{RL}^l T^{e\dagger}$). In models with large $\tan\beta$ the slepton mass eigenstates \tilde{l}_{τ_L} , \tilde{l}_{τ_R} pick substantial contributions from supersymmetric states $\tilde{\tau}_R$, $\tilde{\tau}_L$ respectively. Perturbative expansion of 6×6 matrix \tilde{M}^{l2} on \tilde{M}_{LR}^{l2} , \tilde{M}_{RL}^{l2} sectors is no longer valid. As a consequence full diagonalisation of \tilde{M}^{l2} renders \tilde{S}_{LR}^l (\tilde{S}_{RL}^l) misaligned with S^e (T^e). Chirality flip is suppressed due to small \tilde{M}_{LR}^{l2} , \tilde{M}_{RL}^{l2} but enhanced by diagonal H_{11A} entries. These two factors balance each other and make $A_{R_3} \sim A_{R_2}$ (Figure 4). Lets consider the chargino contribution A_{R_1} . In the large $M_{1/2}$ limit $\tilde{M}_{LL}^{n2} \sim \tilde{M}_{LL}^{l2}$ and $J \sim H \Rightarrow |A_{R_1}| \sim |A_{R_2}| \sim |A_{R_3}|$. All flavour violations are due to $\tilde{T}^L T^{e\dagger} \neq 1$. If $M_{1/2}$ is not too big, A_{R_1} is enhanced because \tilde{S}_{LL}^n becomes between \tilde{T}^L and T^ν thus increasing $\tilde{S}_{LL}^n T^{e\dagger}$. Numerically we found A_R to depend heavily on A_{R_1} over almost all the parameter space studied (Figure 4).

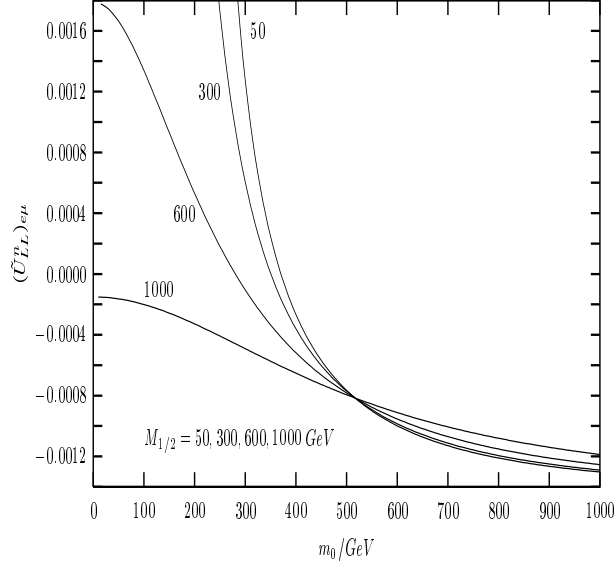


Figure 3. Dependence of $(\tilde{U}_{LL}^n)_{e\mu}$ with the universal Planck scalar mass m_0 for several values of gaugino ($M_{1/2}$) mass. The sudden increase in $(\tilde{U}_{LL}^n)_{e\mu}$ for $M_{1/2} = 50, 300$ GeV near $m_0 \sim 250$ GeV has little physical meaning because it relates to the high degeneracy of the sneutrino spectrum (Figure 8).

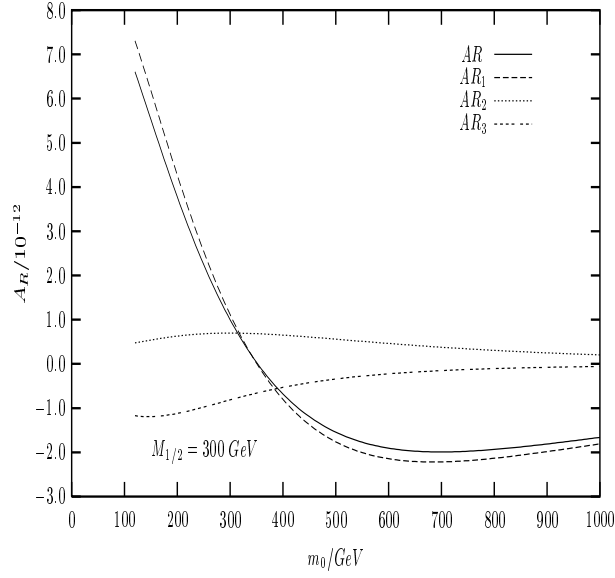


Figure 4. Dependence of dominant amplitudes A_{R_i} with m_0 . It is clear that the neutralino contributions $A_{R_{2,3}}$ can be neglected over almost all m_0 range.

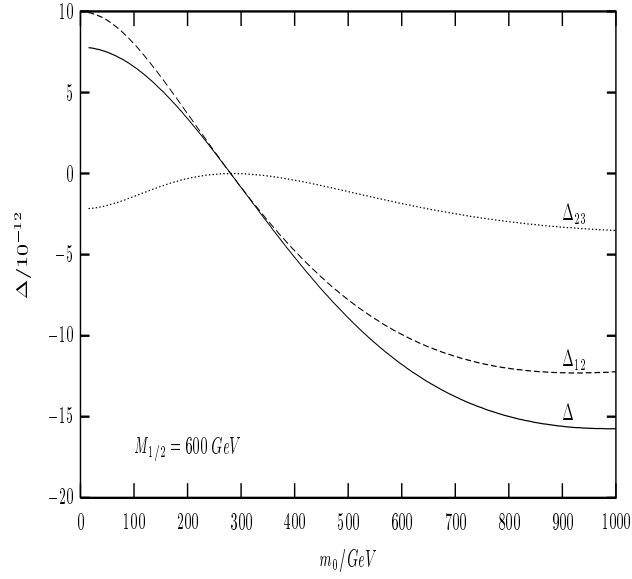


Figure 5. Lepton flavour violation is driven by splitting of masses between the first two families as given by Δ_{12} .

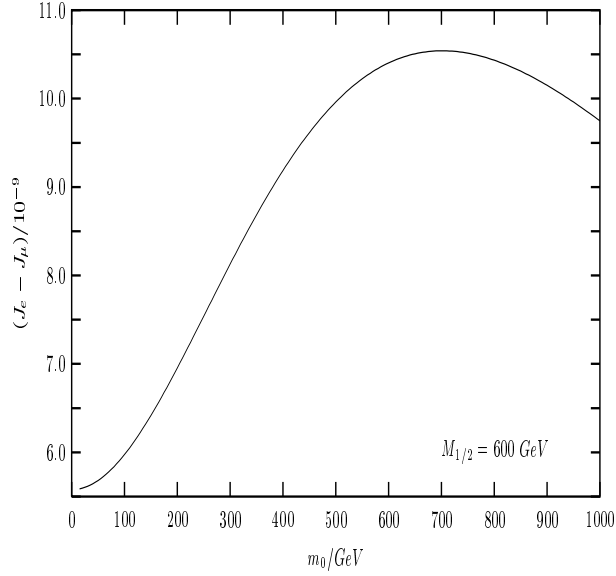


Figure 6. Scaling of $J_e - J_\mu$ function with m_0 .

We now focus on the behaviour of A_{R_1} itself. Defining $\Delta = \text{Const.} \times A_{R_1} = \Delta_{12} + \Delta_{23}$ ($J_A = J_{21A}$ and using approximate unitarity of \tilde{U}_{LL}^n) gives :

$$\Delta_{12} = -(\tilde{U}_{LL}^{n\dagger})_{ee}(\tilde{U}_{LL}^n)_{e\mu}(J_e - J_\mu) \quad (28)$$

$$\Delta_{23} = -(\tilde{U}_{LL}^{n\dagger})_{e\tau}(\tilde{U}_{LL}^n)_{\tau\mu}(J_\mu - J_\tau) \quad (29)$$

The above results allow a direct interpretation of LFV in terms of $e-\mu$, $\mu-\tau$ splittings in Figure 5 and $J_e - J_\mu$ whose scaling with m_0 is shown in Figure 6. If $\tan\beta$ is small then $|\Delta_{23}| \gg |\Delta_{12}|$, while as Figure 5 shows for large $\tan\beta$ over much of parameter space we find $|\Delta_{12}| \gg |\Delta_{23}|$. The empirical effect we observe seems to be related to the large $\tan\beta$ result that $\lambda_\mu \gg \lambda_{charm}$, which tells us that second family Yukawa couplings receive an overall enhancement and this is responsible for the increase in 12 family splittings. It turns out that the 23 family mixing is also substantially increased in this model, but for $\mu \rightarrow e + \gamma$ this effect is killed by the small 13 family mixing factor. For $\tau \rightarrow \mu + \gamma$, on the other hand, the rate here is controlled exclusively by 23 family mixing and we find a large enhancement in this case.

4.2 Overview of Results.

In our numerical results we assumed $\alpha_s = 0.115$ and $m_{bottom} = 4.25$ GeV. An increase in α_s (m_{bottom}) leads to smaller slepton masses (bigger $e - \mu$ splitting) therefore to an enhancement of LFV. The parameters we made to vary were $M_{1/2}$, m_0 , A_0 and M_ν . When not explicitly mentioned the graphs refer to default values of $A_0 = 0$ GeV and $M_\nu = M_{GUT}$. In Figure 7 we plotted the slepton spectrum \tilde{m}_l . Due to large $\tan\beta$, for decreasing m_0 , we verify that the lightest slepton \tilde{l}_{τ_R} is rapidly driven negative, on the other hand \tilde{l}_{τ_L} is pushed upwards and forced to be the heaviest sparticle. This phenomena are absent in conventional low $\tan\beta$ models. Figure 8 which displays sneutrino masses \tilde{m}_n is interesting because it shows that we do not always have $\tilde{m}_{n_e} \sim \tilde{m}_{n_\mu} > \tilde{m}_{n_\tau}$. This relation is inverted for low m_0 due to the reverse hierarchies in the matrices \tilde{m}_L and m_ν . The neutralino particle spectrum is shown in Figure 9. ⁷

⁷When $m_0, M_{1/2} > m_Z$, the heaviest chargino is approximately degenerate with the two heaviest neutralinos (which scale with μ , the Higgs mixing parameter), while the lightest chargino has the same mass as the second lightest neutralino (both scale with M_2). Finally the lightest neutralino scales with M_1 . These three sets are in close correspondence with the scaling of Higgsinos, Winos and Bino.

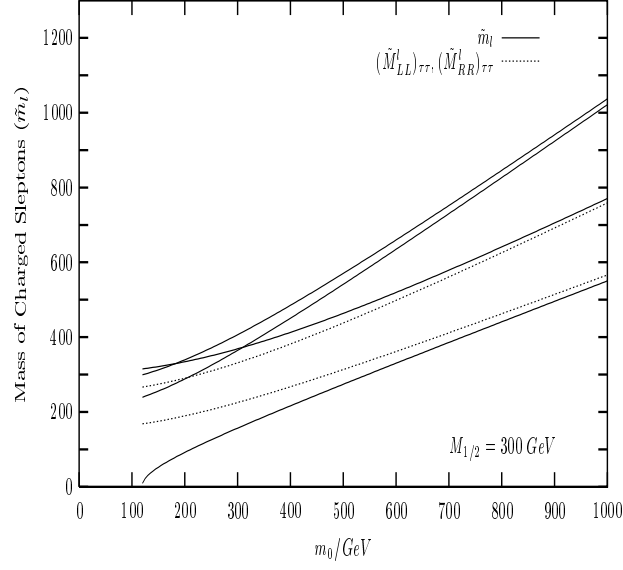


Figure 7. Spectrum of charged sleptons \tilde{l} for a range of m_0 and a selected value of gaugino mass $M_{1/2}$. Mixing between left and right staus is shown as a deviation of the solid line from the dotted one.

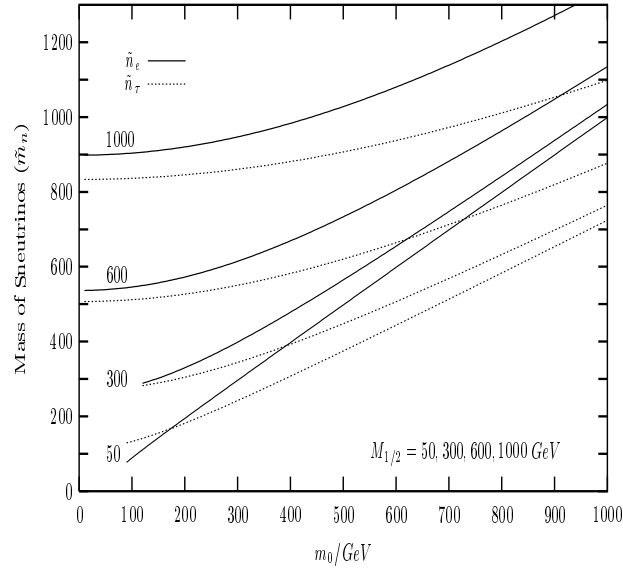


Figure 8. Spectrum of sneutrinos \tilde{n}_e and \tilde{n}_τ as function of m_0 for several values of $M_{1/2}$.

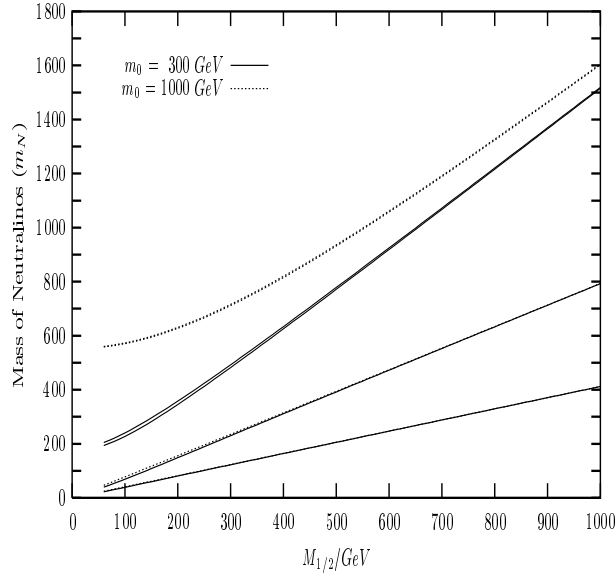


Figure 9. Spectrum of neutralinos as function of $M_{1/2}$.

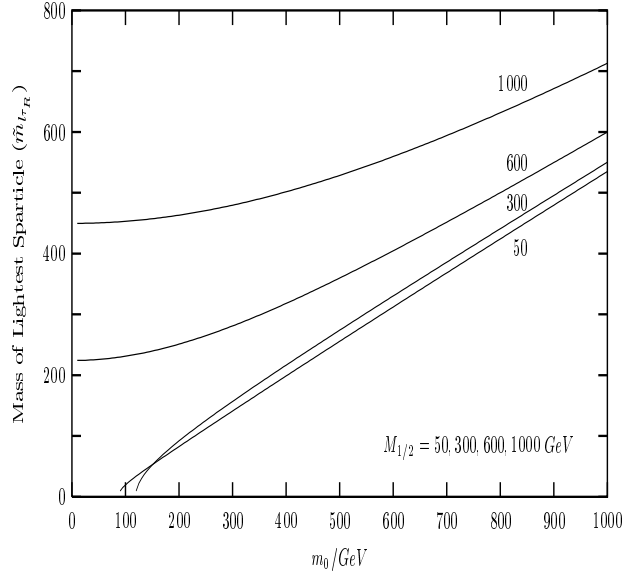


Figure 10. Mass of lightest scalar particle, namely the right-handed stau (\tilde{l}_{τ_R}).

We now consider the branch ratio $\mu \rightarrow e + \gamma$. In Figure 11 we plot its dependence with m_0 for selected values of $M_{1/2}$ (and just two extreme values of M_ν). Discontinued lines signal regions where $\tilde{m}_{l_{\tau_R}} \rightarrow 0$. Generally $\text{BR}(\mu \rightarrow e + \gamma)$ decreases for increasing $M_{1/2}$ and/or m_0 because we are getting heavier sparticles on that limit. However for the lower $M_{1/2}$ values the behaviour is clearly not smooth,

with a resonant inverted spike for particular m_0 values. This behaviour is due to the off-diagonal (flavour-violating) elements of the left-handed sneutrino mass matrix cancelling to zero at particular points in parameter space, and is discussed in more detail in Appendix 5. For $M_{1/2} \leq 800$ GeV one can split the graph into two regions according to m_0 being bigger or smaller than \bar{m}_0 - the value of m_0 at which $A_{R_1} \sim 0$ (\bar{m}_0 itself decreases for increasing $M_{1/2}$). The present experimental bound $\text{BR}(\mu \rightarrow e + \gamma) < 4.9 \times 10^{-11}$ already excludes regions of low $(M_{1/2}, m_0) < (50, 150)$ GeV. The fact that A_{R_1} can be ~ 0 makes this model hard to be excluded as a possible GUT candidate because even if the experimental limit on the branch ratio value gets as low as 10^{-16} one can still argue that we have a very predictive model ⁸.

Figure 12 gives the branch ratio dependence on M_ν , the variations being due to the presence (absence) of right-handed sneutrinos in MSSM+ ν (MSSM) above (below) M_ν . The variations with A_0 are plotted in Figure 13. When $\tan \beta$ is big the sparticles mass matrix is explicit independent of $\tilde{\lambda}_{e,\nu}$. Since RGEs care only about $\tilde{\lambda}_{e,\nu}^2$ we see that the results must be approximately invariant under $A_0 \rightarrow -A_0$. For that reason we have only considered $A_0 > 0$. If $M_{1/2} > 400$ GeV the branch ratio changes only slightly with A_0 . For $M_{1/2} = 300, 400$ GeV increasing A_0 drives A_{R_1} to flip its sign, which actually happens for the former case and doesn't for the latter due to the vanishing of \tilde{l}_{τ_R} mass.

In Figure 14 we show the $\text{BR}(\tau \rightarrow \mu + \gamma)$ which is experimentally constrained to be less than 4.2×10^{-6} . This limit demands, for light $M_{1/2} < 50$ GeV even heavier SUSY particles than the ones imposed by $\mu \rightarrow e + \gamma$. For $M_{1/2}$ around/less 50 GeV we find $m_0 > 220$ GeV. On the other hand, in the heavier $M_{1/2} > 500$ GeV extreme, a severe improvement of experimental accuracy (combined with continued undetection of SUSY sparticles) leads to an upper bound for m_0 around 350 GeV.

⁸This is not unique to 422, SU(5) also shares this kind of behaviour [23], though for a different reason.

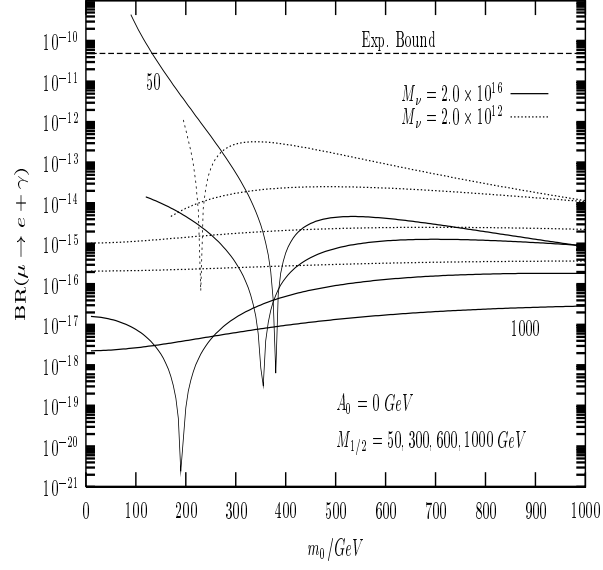


Figure 11. Branch ratio for the decay $\mu \rightarrow e + \gamma$ as function of m_0 for several values of $M_{1/2}$ and two M_ν scales.

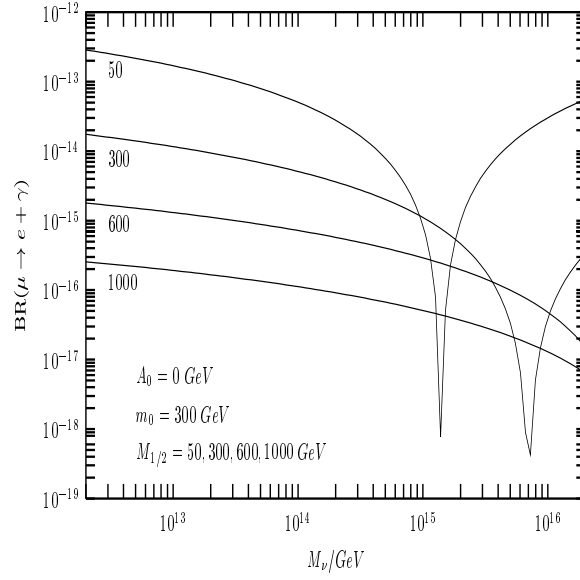


Figure 12. Branch ratio for $\mu \rightarrow e + \gamma$ versus M_ν .

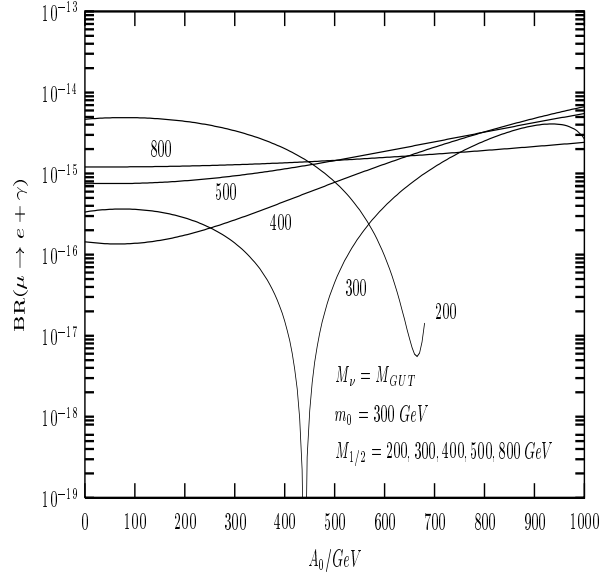


Figure 13. Branch ratio of $\mu \rightarrow e + \gamma$ as function of A_0 .

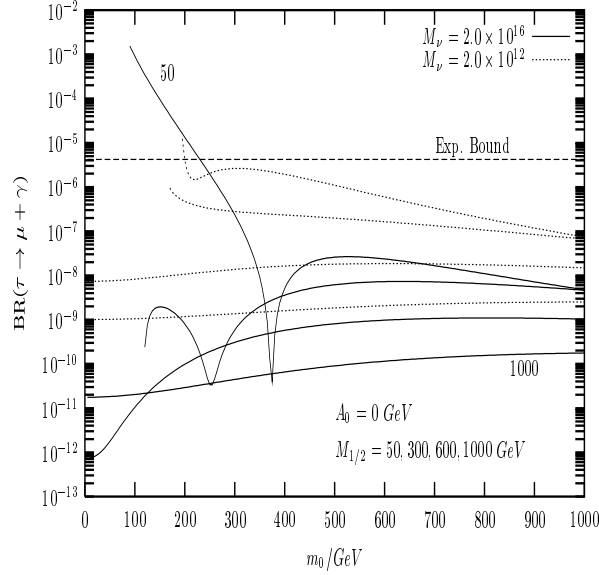


Figure 14. Branch Ratio of $\tau \rightarrow \mu + \gamma$ for a range of m_0 and several values of $M_{1/2}$.

4.3 Results Near the Experimental Limits.

It is clear from the results so far that the interesting region of parameter space from the point of view of the LFV processes corresponds to relatively low values of soft SUSY

breaking parameters, say $m_0 < 500$ GeV and $M_{1/2} < 200$ GeV. In this subsection we shall concentrate on this region, and examine the relationship between LFV processes and direct experimental bounds on the particle mass limits coming from LEP, for example.

In Figure 15 we show the branch ratio for $\mu \rightarrow e + \gamma$ for a range of $m_0 < 500$ GeV and several values of $M_{1/2} < 200$ GeV, taking two extreme values of right-handed neutrino mass. As the experimental bound improves it is clear how increasingly larger regions of the $m_0 - M_{1/2}$ plane in this model may be excluded, with the low values of right-handed neutrino mass (well motivated from neutrino physics) providing the larger rates closer to the experimental limit.

Figure 16 shows the predicted branch ratio for $\tau \rightarrow \mu + \gamma$. The well-motivated $M_\nu = 2 \times 10^{12}$ GeV curves are quite close to the experimental limit, which if increased by an order of magnitude could provide a decisive test of this model.

Figure 17 shows the dependence of $\tau \rightarrow \mu + \gamma$ on the right-hand neutrino scale- M_ν . One can see that, as M_ν decreases, the right-handed neutrino decouples at a lower energy, therefore allowing additional LFV to be generated through the RGE running, which leads to an enhancement in the branch ratio. This effect becomes so strong at low M_ν that it overcomes the other competing source of LFV (see Appendix 5). As a consequence, the inverted peak becomes less pronounced and broader while at the same time steadily moves to lower m_0 until it becomes indistinguishable.

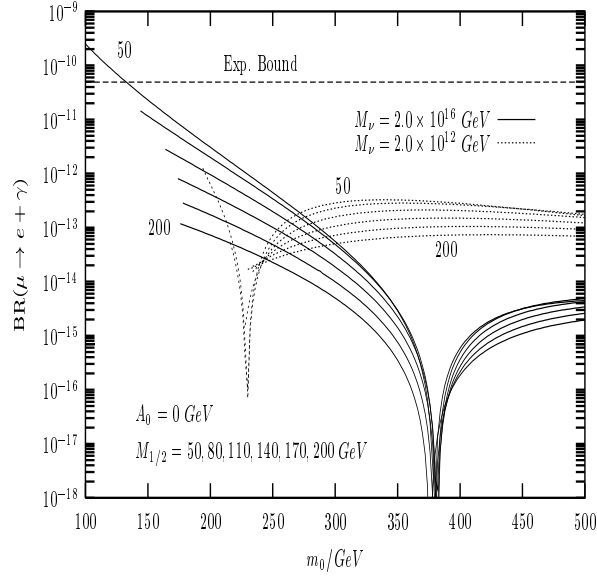


Figure 15. Branch ratio for $\mu \rightarrow e + \gamma$ for a range of $m_0 < 500$ GeV and several values of $M_{1/2} < 200$ GeV. Two extreme values of M_ν are displayed : solid lines correspond to $M_\nu = M_{GUT}$, while dotted lines to $M_\nu = 2 \times 10^{12}$ GeV.

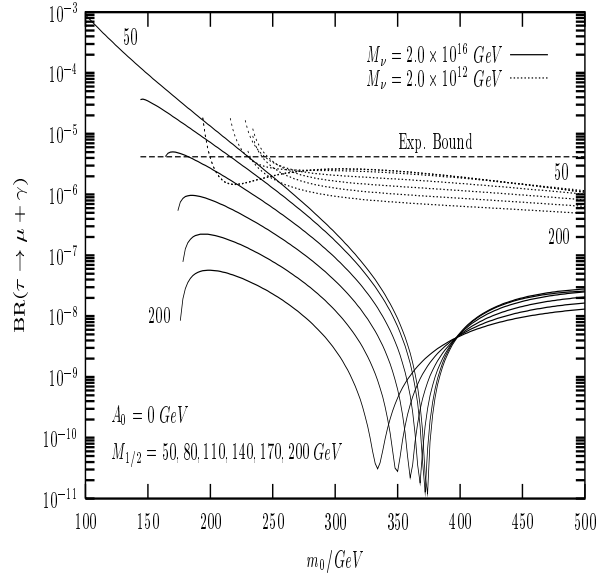


Figure 16. Branch ratio for $\tau \rightarrow \mu + \gamma$ for a range of $m_0 < 500$ GeV and several values of $M_{1/2} < 200$ GeV. Two extreme values of M_ν are displayed : solid lines correspond to $M_\nu = M_{GUT}$, while dotted lines to $M_\nu = 2 \times 10^{12}$ GeV.

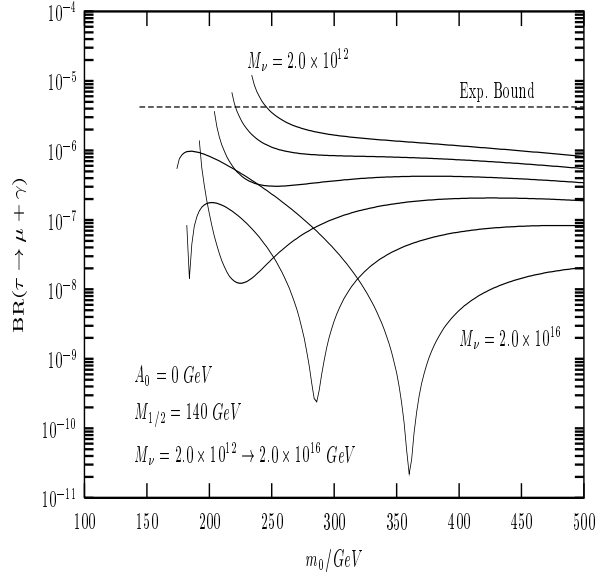


Figure 17. Branch ratio for $\tau \rightarrow \mu + \gamma$ for a range of $m_0 < 500$ GeV and $M_{1/2} = 140$ GeV. The six curves plotted correspond to equally log-scaled intervals of M_ν in the range 2×10^{12} to 2×10^{16} .

In this model the spectrum is completely determined by the values of the input parameters, in particular m_0 and $M_{1/2}$, with very little sensitivity to M_ν for example. It is clearly of interest to compare the direct experimental limits which may be placed on these parameters, from LEP for example, to the indirect limits coming from the LFV processes we have considered. Therefore we present a series of plots which give a detailed exposition of the sparticle spectrum in the low mass region where experiments are sensitive to LFV processes.

We begin in Figure 18 by showing the spectrum of charged sleptons for a fixed low value of $M_{1/2} = 140$ GeV corresponding to charginos in the unexplored LEP2 range 95-105 GeV (as we shall see shortly). The plot shows that the lightest charged slepton mass ranges from 75-250 GeV over the region of $m_0 = 215 - 500$ GeV allowed in a scenario in which the LFV bound for the τ decay has improved to 4.2×10^{-7} GeV. Figure 19 shows the very weak dependence of the lightest slepton mass on $M_{1/2}$. The corresponding sneutrino masses in Figure 20 have a similar mass dependence but

are somewhat heavier.

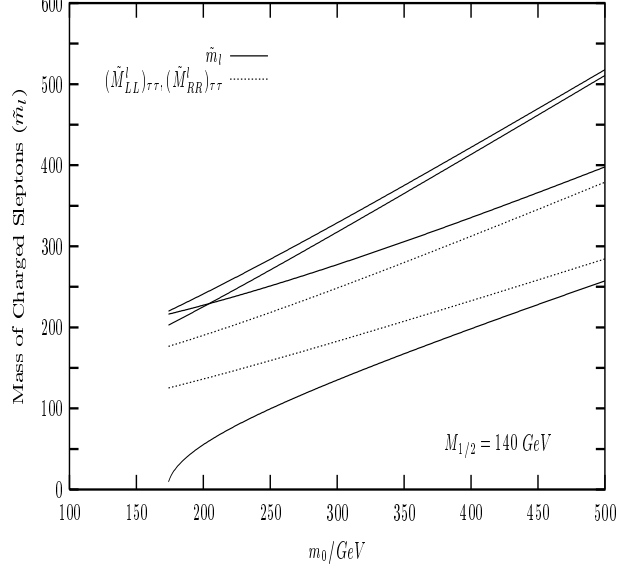


Figure 18. Spectrum of charged sleptons (\tilde{l}) for a range of m_0 and a fixed low value of $M_{1/2} = 140$ GeV. Mixing between left and right staus is shown as a deviation of the solid from the dotted one ($A_0 = 0$ GeV, $M_\nu = 2.0 \times 10^{16}$ GeV).

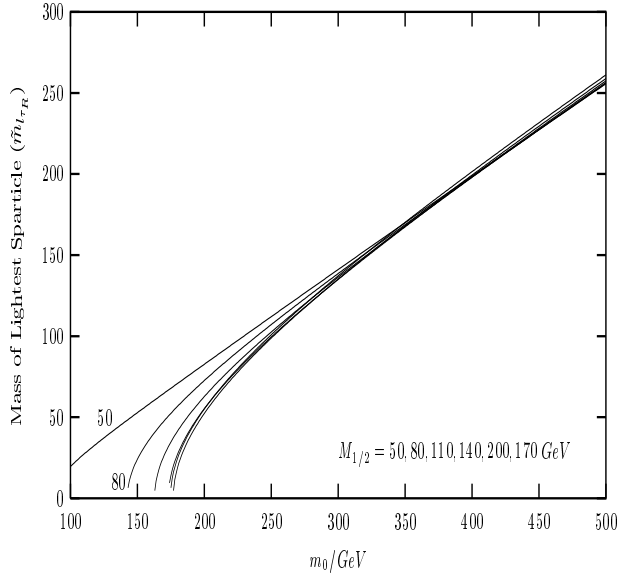


Figure 19. Mass of lightest sparticle, namely the right-handed stau ($\tilde{l}_{\tau R}$), for a range of $m_0 < 500$ GeV and several values of $M_{1/2}$ (Note that the ordering of the $M_{1/2}$ lines which are plotted, from left to right, are in correspondence with the order shown on the label in the graph).

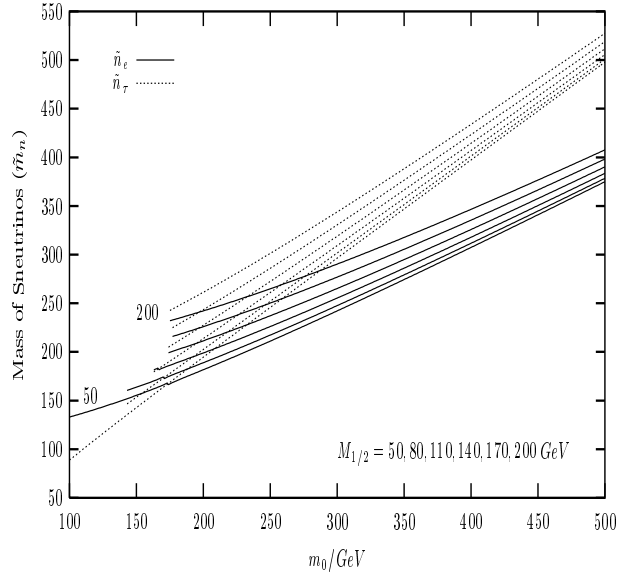


Figure 20. Spectrum of sneutrinos \tilde{n}_e and \tilde{n}_τ for a range of $m_0 < 500$ GeV and several values of $M_{1/2}$ ($A_0 = 0$ GeV, $M_\nu = 2.0 \times 10^{16}$ GeV).

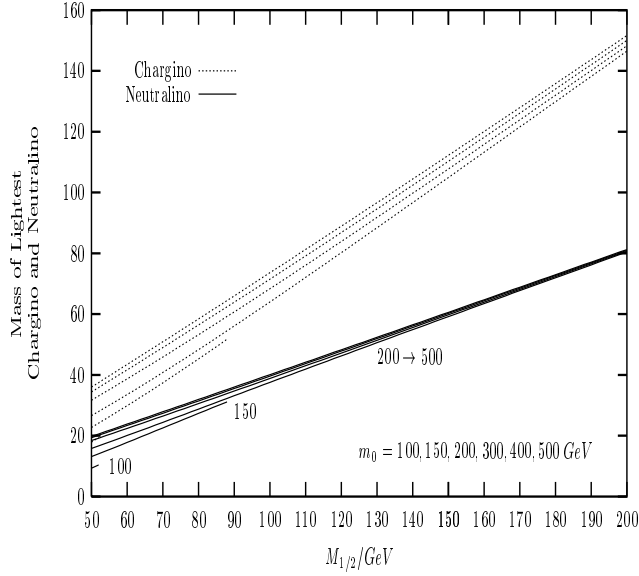


Figure 21. Spectrum of lightest chargino and neutralino for a range of $M_{1/2}$ and selected values of $m_0 < 500$ GeV ($A_0 = 0$ GeV, $M_\nu = 2.0 \times 10^{16}$ GeV).

The strongest constraint on $M_{1/2}$ comes from the lightest charginos and neutralinos in Figure 21. The full spectrum of charginos and neutralinos, for a fixed value of $m_0 = 300$ GeV, and varying $M_{1/2}$, is shown in Figure 22.

The current published LEP2 limit on chargino masses is around 85 GeV [25, 26, 27, 28]. This bound does not include analysis of the most recent runs, which will increase this limit to about 91 GeV. A chargino mass limit of 91 GeV would correspond to $M_{1/2} > 125$ GeV for m_0 in the intermediate 200 – 500 GeV range. The experimental limit on $\tau \rightarrow \mu + \gamma$ would need to be increased by one or two orders of magnitude in order to be competitive with these direct limits.

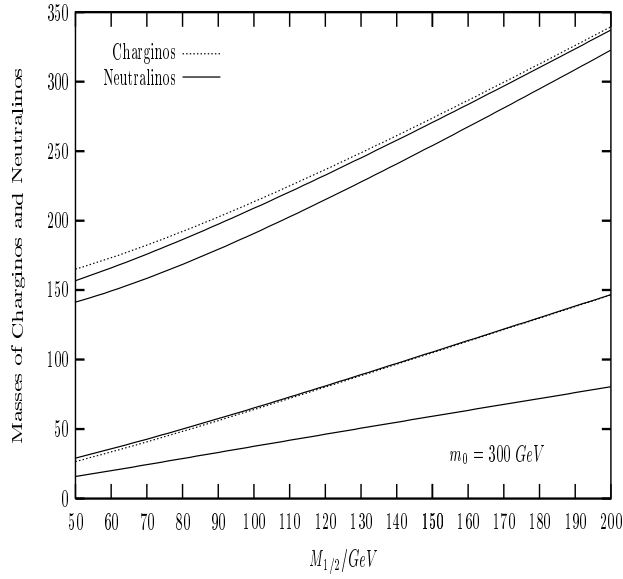


Figure 22. Spectrum of charginos (m_C) and neutralinos (m_N) for a range of $M_{1/2}$ and $m_0 = 300$ GeV ($A_0 = 0$ GeV, $M_\nu = 2.0 \times 10^{16}$ GeV).

5 Conclusions

The main qualitative conclusion of this study is that LFV is not a unique prediction of SUSY GUTs, but is also found in certain string-inspired models which do not possess a simple gauge group. In order to illustrate this we have calculated the minimum irreducible contributions to LFV in a string-inspired minimal $SU(4) \otimes SU(2)_L \otimes SU(2)_R$ model. The main features of this model are large $\tan \beta$ and neutrino masses with an intermediate mass scale M_ν . The mechanism responsible for LFV in the 422 model is similar to the one in MSSM+ ν but here involves a much more constrained

parameter space, leading to a range of $\tan\beta$ outside that previously considered. Also previous studies on the fermion mass spectrum in this model lead to a set of well defined mixing angles which enable precise predictions of LFV to be made. The dominant contribution was seen to come from the amplitude A_{R_1} corresponding to sneutrinos and charginos in the loop, with the LFV controlled by the off-diagonal contributions to the left-handed sneutrino mass squared matrix. In Appendix 5 we saw that the positive off-diagonal contribution from the F-term neutrino mass must compete with the contribution arising from high energy RGE running effects in the high energy region between M_{Planck} and M_ν which is negative and tends to cancel the F-term. The combined effect of these two terms is largely responsible for the resonant suppression of the rates for $\mu \rightarrow e + \gamma$ and $\tau \rightarrow \mu + \gamma$ seen in Figures 11 to 14.

The main quantitative conclusion is that the LFV rates in these models are *substantially enhanced* compared to other models. This conclusion is based on values of mixing angles taken from previous studies of the fermion mass spectrum in this model. The enhancement effect is well illustrated by the detailed analysis of the parameter space near the current experimental limits given in Figures 15 to 22. In particular we find that the current limit on $\tau \rightarrow \mu + \gamma$ is very close to the predictions of this model, especially for the lower values of right-handed neutrino masses which are well motivated by the physics of neutrino masses. If the experimental bounds on $\tau \rightarrow \mu + \gamma$ were improved by one order of magnitude then this model would become severely constrained, providing a decisive test of such models. Since we have concentrated on the *minimum irreducible* amount of LFV in the model, failure to observe $\tau \rightarrow \mu + \gamma$ at its predicted rate would enable such models to be experimentally excluded. More optimistically a direct observation of $\tau \rightarrow \mu + \gamma$ could provide an indirect discovery of supersymmetry in general and large $\tan\beta$ string-inspired models in particular.

Appendix 1: Effective Theory Below M_{PS} .

Below the 422 breaking scale $M_{PS} \sim 10^{16}$ GeV, the model effectively reduces to the MSSM+ ν model. The effective Lagrangian is given by summing the superpotential, scalar potential, scalar and gaugino mass contributions $\mathcal{L} = \mathcal{L}_W - \mathcal{V} - \mathcal{L}_m - \mathcal{L}_\lambda$, each of which we have written in the following form :

$$\begin{aligned} \mathcal{W} = & u^c \lambda_u Q H_u + d^c \lambda_d Q H_d + \\ & \nu^c \lambda_\nu L H_u + e^c \lambda_e L H_d + \mu H_u H_d + 1/2 M_\nu \nu^c \nu^c \end{aligned} \quad (30)$$

$$\begin{aligned} \mathcal{V} = & \tilde{u}^c \tilde{\lambda}_u \tilde{Q} H_u + \tilde{d}^c \tilde{\lambda}_d \tilde{Q} H_d + \\ & \tilde{\nu}^c \tilde{\lambda}_\nu \tilde{L} H_u + \tilde{e}^c \tilde{\lambda}_e \tilde{L} H_d + \tilde{\mu}^2 H_u H_d + \text{h.c.} \end{aligned} \quad (31)$$

$$\begin{aligned} \mathcal{L}_m = & m_{H_u}^2 |H_u|^2 + m_{H_d}^2 |H_d|^2 + \\ & \tilde{Q}^\dagger \tilde{m}_Q^2 \tilde{Q} + \tilde{u}^c \tilde{m}_{u^c}^2 \tilde{u}^{c\dagger} + \tilde{d}^c \tilde{m}_{d^c}^2 \tilde{d}^{c\dagger} + \\ & \tilde{L}^\dagger \tilde{m}_L^2 \tilde{L} + \tilde{\nu}^c \tilde{m}_{\nu^c}^2 \tilde{\nu}^{c\dagger} + \tilde{e}^c \tilde{m}_{e^c}^2 \tilde{e}^{c\dagger} \end{aligned} \quad (32)$$

$$\mathcal{L}_\lambda = 1/2 M_1 \overline{\tilde{B}} \tilde{B} + 1/2 M_2 \overline{\tilde{W}_a} \tilde{W}_a + 1/2 M_3 \overline{\tilde{G}_x} \tilde{G}_x \quad (33)$$

which defines our conventions and notation for the soft parameters in the low energy effective theory.

Appendix 2: RGEs.

This appendix lists the one loop RGEs which we used to run the parameters between M_{GUT} and M_{Planck} using the effective 422 model as described in Section 3. We have neglected the wave function renormalization of the GUT Higgs fields, consequently the equations resemble those of the MSSM+ ν with effective Yukawa

couplings $\lambda_u, \lambda_d, \lambda_\nu, \lambda_e$, but with the $SU(4) \otimes SU(2)_L \otimes SU(2)_R$ gauge group instead of the standard model gauge group.

- The gauge group factors are given by :

Group	i	b_i	c_i^λ	c_i^h	c_i^{2h}	c_i^F	$c_i^{F^c}$
$SU(4)$	1	-6	15/4	0	0	15/8	15/8
$SU(2)_L$	2	1	3/2	3/4	3/2	3/4	0
$SU(2)_R$	3	1	3/2	3/4	3/2	0	3/4

The b s displayed above account only for the contributions coming from the F, F^c and h multiplets. More generally one can write :

$$(b_4, b_L, b_R) = (-6, 1, 1) + 2n_{H_L}(1, 2, 0) + 2n_{H_R}(1, 0, 2) + n_D(1, 0, 0)$$

Where the second term refers to n_{H_L} copies of the Higgs H, H^c as in (5), the third for n_{H_R} copies of GUT Higgs H_R, H_R^c in $(4, 2, 1), (\bar{4}, \bar{2}, 1)$ and the last for n_D copies of D sextet fields in $(6, 1, 1)$. These extra fields are necessary in order to guarantee that the gauge couplings remain unified above M_{PS} [15].

- Running of gauge couplings and gauginos :

$$16\pi^2 \frac{dg_i}{dt} = b_i g_i^3 \quad 16\pi^2 \frac{dM_i}{dt} = 2b_i M_i g_i^2$$

- Running of superpotential Yukawa couplings :

$$\begin{aligned} 16\pi^2 \frac{d\lambda_u}{dt} &= \lambda_u [3 \text{tr}\{\lambda_u^\dagger \lambda_u\} + \text{tr}\{\lambda_\nu^\dagger \lambda_\nu\} + 3\lambda_u^\dagger \lambda_u + \lambda_d^\dagger \lambda_d - 2 c_i^\lambda g_i^2] \\ 16\pi^2 \frac{d\lambda_d}{dt} &= \lambda_d [3 \text{tr}\{\lambda_d^\dagger \lambda_d\} + \text{tr}\{\lambda_e^\dagger \lambda_e\} + 3\lambda_d^\dagger \lambda_d + \lambda_u^\dagger \lambda_u - 2 c_i^\lambda g_i^2] \\ 16\pi^2 \frac{d\lambda_\nu}{dt} &= \lambda_\nu [3 \text{tr}\{\lambda_u^\dagger \lambda_u\} + \text{tr}\{\lambda_\nu^\dagger \lambda_\nu\} + 3\lambda_\nu^\dagger \lambda_\nu + \lambda_e^\dagger \lambda_e - 2 c_i^\lambda g_i^2] \\ 16\pi^2 \frac{d\lambda_e}{dt} &= \lambda_e [3 \text{tr}\{\lambda_d^\dagger \lambda_d\} + \text{tr}\{\lambda_e^\dagger \lambda_e\} + 3\lambda_e^\dagger \lambda_e + \lambda_\nu^\dagger \lambda_\nu - 2 c_i^\lambda g_i^2] \end{aligned}$$

- Running of Higgs parameter :

$$16\pi^2 \frac{d\mu}{dt} = \mu [3 \text{tr}\{\lambda_u^\dagger \lambda_u\} + 3 \text{tr}\{\lambda_d^\dagger \lambda_d\} + \text{tr}\{\lambda_\nu^\dagger \lambda_\nu\} + \text{tr}\{\lambda_e^\dagger \lambda_e\} - 2 c_i^{2h} g_i^2]$$

- Running of soft trilinear Yukawa couplings :

$$\begin{aligned}
16\pi^2 \frac{d\tilde{\lambda}_u}{dt} &= \tilde{\lambda}_u [3 \text{tr}\{\lambda_u^\dagger \lambda_u\} + \text{tr}\{\lambda_\nu^\dagger \lambda_\nu\} + 5\lambda_u^\dagger \lambda_u + \lambda_d^\dagger \lambda_d - 2 c_i^\lambda g_i^2] + \\
&\quad 2\lambda_u [3 \text{tr}\{\lambda_u^\dagger \tilde{\lambda}_u\} + \text{tr}\{\lambda_\nu^\dagger \tilde{\lambda}_\nu\} + 2\lambda_u^\dagger \tilde{\lambda}_u + \lambda_d^\dagger \tilde{\lambda}_d + 2 c_i^\lambda M_i g_i^2] \\
16\pi^2 \frac{d\tilde{\lambda}_d}{dt} &= \tilde{\lambda}_d [3 \text{tr}\{\lambda_d^\dagger \lambda_d\} + \text{tr}\{\lambda_e^\dagger \lambda_e\} + 5\lambda_d^\dagger \lambda_d + \lambda_u^\dagger \lambda_u - 2 c_i^\lambda g_i^2] + \\
&\quad 2\lambda_d [3 \text{tr}\{\lambda_d^\dagger \tilde{\lambda}_d\} + \text{tr}\{\lambda_e^\dagger \tilde{\lambda}_e\} + 2\lambda_d^\dagger \tilde{\lambda}_d + \lambda_u^\dagger \tilde{\lambda}_u + 2 c_i^\lambda M_i g_i^2] \\
16\pi^2 \frac{d\tilde{\lambda}_\nu}{dt} &= \tilde{\lambda}_\nu [3 \text{tr}\{\lambda_u^\dagger \lambda_u\} + \text{tr}\{\lambda_\nu^\dagger \lambda_\nu\} + 5\lambda_\nu^\dagger \lambda_\nu + \lambda_e^\dagger \lambda_e - 2 c_i^\lambda g_i^2] + \\
&\quad 2\lambda_\nu [3 \text{tr}\{\lambda_u^\dagger \tilde{\lambda}_u\} + \text{tr}\{\lambda_\nu^\dagger \tilde{\lambda}_\nu\} + 2\lambda_\nu^\dagger \tilde{\lambda}_\nu + \lambda_e^\dagger \tilde{\lambda}_e + 2 c_i^\lambda M_i g_i^2] \\
16\pi^2 \frac{d\tilde{\lambda}_e}{dt} &= \tilde{\lambda}_e [3 \text{tr}\{\lambda_d^\dagger \lambda_d\} + \text{tr}\{\lambda_e^\dagger \lambda_e\} + 5\lambda_e^\dagger \lambda_e + \lambda_\nu^\dagger \lambda_\nu - 2 c_i^\lambda g_i^2] + \\
&\quad 2\lambda_e [3 \text{tr}\{\lambda_d^\dagger \tilde{\lambda}_d\} + \text{tr}\{\lambda_e^\dagger \tilde{\lambda}_e\} + 2\lambda_e^\dagger \tilde{\lambda}_e + \lambda_\nu^\dagger \tilde{\lambda}_\nu + 2 c_i^\lambda M_i g_i^2]
\end{aligned}$$

- Running of soft Higgs parameter :

$$\begin{aligned}
16\pi^2 \frac{d\tilde{\mu}^2}{dt} &= \tilde{\mu}^2 [3 \text{tr}\{\lambda_u^\dagger \lambda_u\} + 3\text{tr}\{\lambda_d^\dagger \lambda_d\} + \text{tr}\{\lambda_\nu^\dagger \lambda_\nu\} + \text{tr}\{\lambda_e^\dagger \lambda_e\} - 2 c_i^{2h} g_i^2] + \\
&\quad 2\mu [3 \text{tr}\{\lambda_u^\dagger \tilde{\lambda}_u\} + 3\text{tr}\{\lambda_d^\dagger \tilde{\lambda}_d\} + \text{tr}\{\lambda_\nu^\dagger \tilde{\lambda}_\nu\} + \text{tr}\{\lambda_e^\dagger \tilde{\lambda}_e\} + 2 c_i^{2h} M_i g_i^2]
\end{aligned}$$

- Running of soft scalar masses :

$$\begin{aligned}
16\pi^2 \frac{d\tilde{m}_Q^2}{dt} &= [\tilde{m}_Q^2 \lambda_u^\dagger \lambda_u + \lambda_u^\dagger (m_{H_u}^2 + \tilde{m}_{u^c}^2) \lambda_u + \tilde{\lambda}_u^\dagger \tilde{\lambda}_u + \\
&\quad \tilde{m}_Q^2 \lambda_d^\dagger \lambda_d + \lambda_d^\dagger (m_{H_d}^2 + \tilde{m}_{d^c}^2) \lambda_d + \tilde{\lambda}_d^\dagger \tilde{\lambda}_d + \text{h.c.}] - 8 c_i^F M_i^2 g_i^2 \\
16\pi^2 \frac{d\tilde{m}_{u^c}^2}{dt} &= 2 [\tilde{m}_{u^c}^2 \lambda_u \lambda_u^\dagger + \lambda_u (m_{H_u}^2 + \tilde{m}_Q^2) \lambda_u^\dagger + \tilde{\lambda}_u \tilde{\lambda}_u^\dagger + \text{h.c.}] - 8 c_i^{Fc} M_i^2 g_i^2 \\
16\pi^2 \frac{d\tilde{m}_{d^c}^2}{dt} &= 2 [\tilde{m}_{d^c}^2 \lambda_d \lambda_d^\dagger + \lambda_d (m_{H_d}^2 + \tilde{m}_Q^2) \lambda_d^\dagger + \tilde{\lambda}_d \tilde{\lambda}_d^\dagger + \text{h.c.}] - 8 c_i^{Fc} M_i^2 g_i^2 \\
16\pi^2 \frac{d\tilde{m}_L^2}{dt} &= [\tilde{m}_L^2 \lambda_\nu^\dagger \lambda_\nu + \lambda_\nu^\dagger (m_{H_u}^2 + \tilde{m}_{\nu^c}^2) \lambda_\nu + \tilde{\lambda}_\nu^\dagger \tilde{\lambda}_\nu + \\
&\quad \tilde{m}_L^2 \lambda_e^\dagger \lambda_e + \lambda_e^\dagger (m_{H_d}^2 + \tilde{m}_{e^c}^2) \lambda_e + \tilde{\lambda}_e^\dagger \tilde{\lambda}_e + \text{h.c.}] - 8 c_i^F M_i^2 g_i^2 \\
16\pi^2 \frac{d\tilde{m}_{\nu^c}^2}{dt} &= 2 [\tilde{m}_{\nu^c}^2 \lambda_\nu \lambda_\nu^\dagger + \lambda_\nu (m_{H_u}^2 + \tilde{m}_L^2) \lambda_\nu^\dagger + \tilde{\lambda}_\nu \tilde{\lambda}_\nu^\dagger + \text{h.c.}] - 8 c_i^{Fc} M_i^2 g_i^2 \\
16\pi^2 \frac{d\tilde{m}_{e^c}^2}{dt} &= 2 [\tilde{m}_{e^c}^2 \lambda_e \lambda_e^\dagger + \lambda_e (m_{H_d}^2 + \tilde{m}_L^2) \lambda_e^\dagger + \tilde{\lambda}_e \tilde{\lambda}_e^\dagger + \text{h.c.}] - 8 c_i^{Fc} M_i^2 g_i^2
\end{aligned}$$

- Running of Higgs masses :

$$16\pi^2 \frac{dm_{H_u}^2}{dt} = 6 \text{tr}\{ \tilde{m}_Q^2 \lambda_u^\dagger \lambda_u + \lambda_u^\dagger (m_{H_u}^2 + \tilde{m}_{u^c}^2) \lambda_u + \tilde{\lambda}_u^\dagger \tilde{\lambda}_u \} +$$

$$\begin{aligned}
& 2 \operatorname{tr}\{\tilde{m}_L^2 \lambda_\nu^\dagger \lambda_\nu + \lambda_\nu^\dagger (m_{H_u}^2 + \tilde{m}_{\nu^c}^2) \lambda_\nu + \tilde{\lambda}_\nu^\dagger \tilde{\lambda}_\nu\} - 8 c_i^h M_i^2 g_i^2 \\
16\pi^2 \frac{dm_{H_d}^2}{dt} = & 6 \operatorname{tr}\{\tilde{m}_Q^2 \lambda_d^\dagger \lambda_d + \lambda_d^\dagger (m_{H_d}^2 + \tilde{m}_{d^c}^2) \lambda_d + \tilde{\lambda}_d^\dagger \tilde{\lambda}_d\} + \\
& 2 \operatorname{tr}\{\tilde{m}_L^2 \lambda_e^\dagger \lambda_e + \lambda_e^\dagger (m_{H_d}^2 + \tilde{m}_{e^c}^2) \lambda_e + \tilde{\lambda}_e^\dagger \tilde{\lambda}_e\} - 8 c_i^h M_i^2 g_i^2
\end{aligned}$$

Appendix 3: Diagonalisation of Mass Matrices.

The soft trilinear Yukawa couplings and mass terms of the 422 theory are $\tilde{F}^c \tilde{\lambda} \tilde{F} h$ and $\tilde{F}^\dagger \tilde{m}_F^2 \tilde{F}$, $\tilde{F}^c \tilde{m}_{F^c}^2 \tilde{F}^{c\dagger}$. Below the symmetry breaking scale \tilde{m}_F^2 splits into \tilde{m}_Q^2 , \tilde{m}_L^2 , and $\tilde{m}_{F^c}^2$ splits into $\tilde{m}_{u^c}^2$, $\tilde{m}_{d^c}^2, \tilde{m}_{e^c}^2$, $\tilde{m}_{\nu^c}^2$. We now specify how Yukawa and soft scalar mass matrices are diagonalised :

$$S^u \lambda_u T^{u\dagger} = \lambda_u(d) \quad S^d \lambda_d T^{d\dagger} = \lambda_d(d) \quad (34)$$

$$S^\nu \lambda_\nu T^{\nu\dagger} = \lambda_\nu(d) \quad S^e \lambda_e T^{e\dagger} = \lambda_e(d) \quad (35)$$

$$\tilde{T}^Q \tilde{m}_Q^2 \tilde{T}^{Q\dagger} = \tilde{m}_Q^2(d) \quad \tilde{T}^L \tilde{m}_L^2 \tilde{T}^{L\dagger} = \tilde{m}_L^2(d) \quad (36)$$

$$\tilde{S}^{u^c} \tilde{m}_{u^c}^2 \tilde{S}^{u^c\dagger} = \tilde{m}_{u^c}^2(d) \quad \tilde{S}^{d^c} \tilde{m}_{d^c}^2 \tilde{S}^{d^c\dagger} = \tilde{m}_{d^c}^2(d) \quad (37)$$

$$\tilde{S}^{\nu^c} \tilde{m}_{\nu^c}^2 \tilde{S}^{\nu^c\dagger} = \tilde{m}_{\nu^c}^2(d) \quad \tilde{S}^{e^c} \tilde{m}_{e^c}^2 \tilde{S}^{e^c\dagger} = \tilde{m}_{e^c}^2(d) \quad (38)$$

The left-handed neutrinos obtain a small mass $\sim m_\nu^2/4M_\nu$ after diagonalization of :

$$\mathcal{L} = -(\nu \quad \nu^c) \begin{pmatrix} 0 & 1/2 m_\nu^T \\ 1/2 m_\nu & M_\nu \end{pmatrix} \begin{pmatrix} \nu \\ \nu^c \end{pmatrix} + \text{h.c.} \quad (39)$$

We introduce \tilde{S}^n , \tilde{S}^l which diagonalise the 6×6 sneutrino \tilde{M}^{n2} , selectron \tilde{M}^{l2} mass matrices :

$$\begin{aligned}
\tilde{S}^n \tilde{M}^{n2} \tilde{S}^{n\dagger} = \tilde{M}^{n2}(d) \quad \tilde{M}^{n2} = & \begin{pmatrix} \tilde{M}_{LL}^{n2} & \tilde{M}_{LR}^{n2} \\ \tilde{M}_{RL}^{n2} & \tilde{M}_{RR}^{n2} \end{pmatrix} \quad \tilde{S}^n = \begin{pmatrix} \tilde{S}_{LL}^n & \tilde{S}_{LR}^n \\ \tilde{S}_{RL}^n & \tilde{S}_{RR}^n \end{pmatrix} \\
\tilde{S}^l \tilde{M}^{l2} \tilde{S}^{l\dagger} = \tilde{M}^{l2}(d) \quad \tilde{M}^{l2} = & \begin{pmatrix} \tilde{M}_{LL}^{l2} & \tilde{M}_{LR}^{l2} \\ \tilde{M}_{RL}^{l2} & \tilde{M}_{RR}^{l2} \end{pmatrix} \quad \tilde{S}^l = \begin{pmatrix} \tilde{S}_{LL}^l & \tilde{S}_{LR}^l \\ \tilde{S}_{RL}^l & \tilde{S}_{RR}^l \end{pmatrix}
\end{aligned} \quad (40)$$

The left-handed sneutrino mass matrix is given by : ⁹

$$\tilde{M}_{LL}^{n2} = \tilde{m}_L^2 + m_\nu^\dagger m_\nu + m_Z^2 Z_{\nu_L} c_{2\beta} \quad (41)$$

We denote the eigenvalues of \tilde{M}^{n2} and \tilde{M}^{l2} by \tilde{m}_n^2 ($\tilde{m}_{n_A}^2 = \tilde{m}_{n_{A_L}}^2$, $\tilde{m}_{n_{\bar{A}}}^2 = \tilde{m}_{n_{A_R}}^2$) and \tilde{m}_l^2 ($\tilde{m}_{l_A}^2 = \tilde{m}_{l_{A_L}}^2$, $\tilde{m}_{l_{\bar{A}}}^2 = \tilde{m}_{l_{A_R}}^2$) respectively. The \tilde{U} s are given by :

$$\tilde{U}^{n,l} = \begin{pmatrix} \tilde{U}_{LL}^{n,l} & \tilde{U}_{LR}^{n,l} \\ \tilde{U}_{RL}^{n,l} & \tilde{U}_{RR}^{n,l} \end{pmatrix} = \begin{pmatrix} \tilde{S}_{LL}^{n,l} T^{e\dagger} & \tilde{S}_{LR}^{n,l} S^{e\dagger} \\ \tilde{S}_{RL}^{n,l} T^{e\dagger} & \tilde{S}_{RR}^{n,l} S^{e\dagger} \end{pmatrix} \quad (42)$$

Finally we provide the expressions for J and H :

$$J_{ijA} = \sum_{k=1,2} (g_1 S_{ik}^{C\dagger})(g_1 T_{kj}^C) m_{C_k} / \tilde{m}_{n_A}^2 J_{kA} \quad J_{kA} = \mathcal{J}(m_{C_k}^2 / \tilde{m}_{n_A}^2) \quad (43)$$

$$H_{pqA} = \sum_{r=1..4} (g_p S_{pr}^{N\dagger})(g_q S_{rq}^N) m_{N_r} / \tilde{m}_{l_A}^2 H_{rA} \quad H_{rA} = \mathcal{H}(m_{N_r}^2 / \tilde{m}_{l_A}^2) \quad (44)$$

Here $g_{p,q} = (g', g, g, g)$ and the function $\mathcal{J}(\mathcal{H})$ arises from chargino (neutralino) loop integration [6]. The (supersymmetric state) indices i, j, p and q can take values among : $i = (1, 2) = (\tilde{W}_R^-, \tilde{H}_R^-)$, $j = (1, 2) = (\tilde{W}_L^-, \tilde{H}_L^-)$, p and $q = (1, 2, 3, 4) = (\tilde{B}, \tilde{W}^0, \tilde{H}_d^0, \tilde{H}_u^0)$. S^C and T^C diagonalise ($S^C M^C T^{C\dagger} = M^C(d)$) the 2×2 chargino mass matrix M^C which has eigenvalues m_{C_k} . Similarly S^N diagonalises ($S^N M^N S^{N\dagger} = M^N(d)$) the 4×4 neutralino mass matrix M^N which has eigenvalues m_{N_r} .

$$M^C = \begin{pmatrix} M_2 & \sqrt{2} m_W s_\beta \\ \sqrt{2} m_W c_\beta & \mu \end{pmatrix} \quad (45)$$

$$M^N = \begin{pmatrix} M_1 & 0 & -m_Z c_\beta s_\theta & m_Z s_\beta s_\theta \\ 0 & M_2 & m_Z c_\beta c_\theta & -m_Z s_\beta c_\theta \\ -m_Z c_\beta s_\theta & m_Z c_\beta c_\theta & 0 & -\mu \\ m_Z s_\beta s_\theta & -m_Z s_\beta c_\theta & -\mu & 0 \end{pmatrix} \quad (46)$$

⁹Note that the neutrino Dirac masses contribute to the left-handed sneutrino masses even though the right-handed (singlet) neutrino superfield is very heavy $\sim M_\nu$. Such terms arise from the F-terms F_{ν^c} which do not involve the heavy ν^c field. Also note that, since $m_\nu = v_u \lambda_\nu$, we have $m_{\nu_\tau} \sim m_{top}$, therefore for low $m_0, M_{1/2}$ it is not true that $\tilde{m}_L \gg m_\nu$. Furthermore in expression (41) we have neglected terms of order m_ν / M_ν which is perfectly valid (The same however does not apply to the analogous contribution to the mass of left-handed neutrinos, since they are made massive exactly because of left-right mixing through λ_ν).

Appendix 4: Fermion Masses and Mixing Angles.

This appendix is intended to give an overview of fermion masses and mixing angles predicted by this model. Ultimately we have in mind their comparison with the available data. We will focus on the effects associated with the running of the parameters between the weak and GUT scale and their variation with the right-handed neutrino decoupling scale M_ν . For convenience we show below the CKM matrix [24] :

$$V^Q = \begin{pmatrix} 0.9747 - 0.9759 & 0.218 - 0.224 & 0.002 - 0.007 \\ 0.218 - 0.224 & 0.9735 - 0.9751 & 0.032 - 0.054 \\ 0.003 - 0.018 & 0.030 - 0.054 & 0.9985 - 0.9995 \end{pmatrix} \quad (47)$$

The results in Tables 1-4 correspond to input values of $\alpha_s = 0.115$ and $m_{bottom} = 4.25$ GeV. Variations due to different choices of these parameters are significant ¹⁰ and have been partially considered in [18]. Since we worked with one-loop RGE all the tables are independent of the Planck scale parameters m_o , $M_{1/2}$ and A_0 .

Table 1						
M_ν/M_{GUT}	Y^1	Y^{Ad}	Y^B	Y^C	Y^D	Y^{33}
1.0000	0.0110	-0.00032	-0.0151	0.0056	0.0074	0.958
0.0001	0.0131	-0.00038	-0.0194	0.0067	0.0087	1.310

In Table 1, we show the values that the Y operators appearing in equations (11)-(14) take at the GUT scale, for two values of $M_\nu = M_{GUT}$ and $M_\nu = 2 \times 10^{12}$. Operators B and 33 can be seen to be the most sensitive to M_ν .

Table 2	V^Q		V^L	
	Weak	GUT	Weak	GUT
V_{12}	0.2210	0.2210	0.0625	0.0625
V_{11}	0.9752	0.9752	0.9980	0.9980
V_{22}	0.9743	0.9747	0.9974	0.9976
V_{33}	0.9990	0.9995	0.9993	0.9995

¹⁰See for example Figure 1.

In Table 2, we have collected the mixing angles which are approximately insensitive to changes in M_ν and stable relative to RGE effects. We denoted the CKM matrix by V^Q and the leptonic counterpart by V^L ($V_{21} \sim V_{12}$). The Clebsh factors in equations (11)-(14) imply $V_{12}^L \sim V_{12}^Q/4$.¹¹

Table 3				
$M_\nu = M_{GUT}$	Weak		GUT	
V_{AB}^Q	Input	Output	Input	Output
V_{23}^Q	0.0430	0.0430	0.0310	0.0310
V_{32}^Q	0.0429	0.0437	0.0309	0.0315
V_{13}^Q	0.0045	0.0078	0.0032	0.0056
V_{31}^Q	0.0051	0.0019	0.0036	0.0013
V_{AB}^L	Unknown		Unknown	
V_{23}^L		0.0352		0.0315
V_{32}^L		0.0352		0.0315
V_{13}^L		0.0016		0.0014
V_{31}^L		0.0006		0.0005

In Table 3 we include the remaining V^Q and V^L entries not present in Table 2 ($M_\nu = 2 \times 10^{16}$). The reason for the discrimination is threefold. Firstly because we are now confronted with values that are more sensitive to variations in M_ν . For example, taking $M_\nu = 10^{-4} \times M_{GUT}$ effects the values shown to about 7 %. Secondly because the mixings in Table 3 are generally not as stable to RGE effects as the ones in Table 2. And finally because we wanted to call attention to the fact that the values that are actually used when we computed LFV processes, denoted by $\langle \text{Output} \rangle$, are not exactly the same as the ones we have available from experiment $\langle \text{Input} \rangle$. The discrepancy arises when we replace the GUT Yukawa couplings by others parameterized by our set of operators arranged in a successful ‘Texture’.

¹¹It is relevant to note that the Y operators were chosen because they can, not only account for the experimental fermion mass pattern but predict successfully ‘natural’ mixing angles as well. By this we mean that we were careful to select them in such a way that none arises as the residue of an almost complete cancellation of the contributions coming from the up and down Yukawa matrices.

Table 4	m_d 7.8 MeV	m_s 214 MeV	m_t 178-175 GeV
m_{ν_e} 0.2 MeV	m_{ν_μ} 760 MeV	m_{ν_τ} 115-122 GeV	$m_{\nu_\tau}^2/4M_\nu$ $1.6 \cdot 10^{-4}$ eV

Finally in Table 4, we present the predictions for some fermion masses. Whenever two values are shown for the same parameter, the first is associated with $M_\nu = 10^{-4}M_{GUT}$ while the second with $M_\nu = M_{GUT}$. The down (strange) quark has a mass within the $5 - 15$ ($100 - 300$) MeV range quoted in [24]. The m_ν values correspond to the unphysical mass directly obtained from the neutrino Yukawa couplings (for example $m_{\nu_\tau} \sim v_u(\lambda_\nu)_{33}$). On the other hand, the physical mass of the tau-neutrino is correctly obtained after taking into account the see-saw suppression mechanism which forces it to scale as $m_{\nu_\tau}^2/4M_\nu$. In all cases we obtained predictions fairly compatible with experimental data.

Appendix 5: Analysis of Suppression in LFV Decays.

In this appendix we investigate the origin of the suppression in the LFV decays observed in Figures 11-14. In section 4.1 we showed that the amplitude A_{R_1} gave the dominant contribution to the LFV branching ratios (see Figure 4.) Furthermore as shown in Eqs.(28), (29) the LFV due to A_{R_1} is controlled by the off-diagonal elements of the matrices \tilde{U}_{LL}^n which are involved in the diagonalisation of the left-handed sneutrino mass squared matrix (see Appendix 3.) The mass matrix for left-handed sneutrinos was given in equation (41) :

$$\tilde{M}_{LL}^{n2} = \tilde{m}_L^2 + m_\nu^\dagger m_\nu + m_Z^2 Z_{\nu_L} c_{2\beta} \quad (48)$$

In the basis in which charged leptons are diagonal we write

$$T^e \tilde{M}_{LL}^{n2} T^{e\dagger} = (T^e \tilde{T}^{L\dagger}) \tilde{m}_L^2(d) (\tilde{T}^L T^{e\dagger}) + (T^e T^{\nu\dagger}) m_\nu^2(d) (T^\nu T^{e\dagger}) + \dots \quad (49)$$

and one immediately recognises the SUSY $T^e \tilde{T}^{L\dagger}$ and non-SUSY $T^e T^{\nu\dagger}$ mixing matrices reflecting the mismatch between the scalar-fermion (superpartners) and charged-neutral lepton eigen-mass basis respectively, which leads to LFV. As we shall see the LFV contributions coming from \tilde{m}_L^2 and m_ν^2 in (49) add destructively and it is this effect that, for some small regions of the available parameter space, leads to LFV being resonantly suppressed.

Now we would like to make some simple analytic estimate of this effect, which we shall do by examining the off-diagonal contributions to \tilde{M}_{LL}^{n2} which are responsible for flavour-violation. We start by noting that the last term in Eq.(48), being universal, is not relevant to what follows, therefore we concentrate on \tilde{m}_L^2 and m_ν which are responsible for off-diagonal flavour-violating entries in \tilde{M}_{LL}^{n2} . Since $m_\nu = v_u \lambda_\nu$ we can see that its presence in (48) cannot be neglected whenever \tilde{m}_L^2 is driven by low m_0 , $M_{1/2}$. With the help of Appendix 2, we solve approximately the RGE for \tilde{m}_L^2 :

$$\tilde{m}_L^2 \sim m_0^2 - \Delta E [(6 m_0^2 + A_0^2)(\lambda_\nu^\dagger \lambda_\nu + \lambda_e^\dagger \lambda_e) - 8 c M_{1/2}^2 g^2] \quad (50)$$

where $\Delta E = \ln(M_{Planck}/M_\nu)/16\pi^2$. In order to illustrate the origin of the suppression in LFV processes in this model, it is convenient to adopt a set of simplifying assumptions which will make the argument clearer. We start by fixing $A_0 = 0$ and $M_\nu = M_{GUT}$, therefore concentrating only on the Planck scale m_0 , $M_{1/2}$ parameters. Additionally it is useful to consider a basis in which the λ_e coupling is diagonal. This means that all LFV will be accounted by off-diagonal λ_ν entries. Finally we introduce a particularly relevant second order effect in (50) which changes $6 m_0^2 \rightarrow 6 m_0^2 + 8 c M_{1/2}^2 \Delta E g^2$. Hence, we arrive at a more transparent form for (48) which has off-diagonal values given by :

$$\tilde{M}_{LL}^{n2}|_{off-diag} = [v_u^2 - \Delta E (6 m_0^2 + 8 c M_{1/2}^2 \Delta E g^2)] \lambda_\nu^\dagger \lambda_\nu \quad (51)$$

The essential point is that the off-diagonal terms in the matrix contain two contributions: the first from the Dirac neutrino mass matrix squared (arising from the

$F_{\nu c}$ -term contribution to the potential) which contributes *positively*, and the second from the RGE running of the soft mass m_0^2 due to Yukawa corrections in the high energy region between M_{Planck} and M_ν which induce off-diagonal *negative* contributions. Although this expression was obtained in a rudimentary way it can nevertheless account for some qualitative features displayed in Figures 15 and 16. Firstly it sets two distinct possible regions depending on v_u^2 being bigger/smaller than m_0^2 , $M_{1/2}^2$ corresponding to positive/negative values of $(\tilde{M}_{LL}^{n2})_{AB}$ respectively ($A \neq B$). Secondly it confirms that the scale \bar{m}_0^2 at which (51) vanishes, decreases for increasing $M_{1/2}$. Finally it shows that \bar{m}_0^2 is the same for all types of LFV decays, ie independent of the initial and final families involved. However the (over) simplification of the approximations in (51) means that this equation cannot be used to reliably estimate \bar{m}_0^2 or to check the higher sensitivity to $M_{1/2}$ for the tau relative to the muon decay.

References

- [1] R.Barbieri, L.J.Hall, Phys. Lett. **B338**, 212 (1994).
- [2] R.Barbieri, L.J.Hall, Nucl.Phys. **B338**, 212 (1994).
- [3] F.Borzumati and A.Masiero, Phys. Rev. Lett. **57**, 961 (1986);
L.J. Hall, V.A. Kostelecky and S.Raby, Nucl. Phys. **B267**, 415 (1986);
T.Kosmas, G.K.Leontaris and J.D.Vergados, Phys. Lett. **B219**, 457 (1989).
- [4] E.Cremmer, S.Ferrara and J.Scherk, Phys. Lett. **B74**, 61 (1978);
H.P.Nilles, Phys.Rep. **110**, 1 (1984).
- [5] V.Barger, M.S.Berger, P.Ohmann, R.J.N.Philips, hep-ph/9308233.
P.Langacker, N.Polonsky, Phys.Rev. **D49**, 1454 (1994)
G.Kane, C.Kolda, L.Roszkowski, J.Wells, Phys.Rev. **D49**, 6173 (1994)

- N.Polonsky, A.Pomarol, Phys.Rev **D51**, 6532 (1995)
- [6] J.Hisano, T.Moroi, K.Tobe, M.Yamaguchi, Phys.Rev. **D53**, 2442 (1996)
- [7] S. F. King and Q. Shafi, hep-ph/9711288, CERN-TH/97-314,
(to appear in Physics Letters B.)
- [8] J.C.Pati, A.Salam, Phys.Rev. **D10**, 275 (1974).
- [9] I.Antoniadis, G.K.Leontaris, Phys.Lett. **B216**, 333 (1989);
I. Antoniadis, G. K. Leontaris and J. Rizos, Phys. Lett. **B245**, 161 (1990) .
- [10] B.C.Allanach, S.F.King, Nucl.Phys **B459**, 75 (1996).
- [11] N.Arkani-Hamed, H.Cheng, L.J.Hall, hep-ph/9508288.
- [12] G.K. Leontaris, N.D. Tracas NTUA-65-97A, hep-ph/9709510;
G.K. Leontaris, N.D. Tracas NTUA-70/78, hep-ph/9803320.
- [13] H.Arason, D.J.Castano, E.J.Piard, P.Ramond, Phys.Rev. **D47**, 232 (1993).
- [14] V.Barger, M.S.Berger, P.Ohmann, Phys.Rev. **D47**, 1093 (1993).
- [15] S. F. King, Phys. Lett. **B 325**(1994) 129.
- [16] G.Anderson, S.Dimopoulos, L.J.Hall, S.Raby, G.D.Starkman, Phys.Rev. **D49**,
3660 (1994).
- [17] H.Georgi, C.Jarlskog, Phys.Lett. **B89**, 297 (1978).
P.Ramond, R.G.Roberts, G.G.Ross, Nucl.Phys. **B406**, 19 (1993)
L.J.Hall, A.Rasin, Phys.Lett. **B315**, 164 (1993)
- [18] B.C.Allanach, S.F.King, Nucl.Phys **B456**, 57 (1995).
- [19] B.C.Allanach, S.F.King, Phys.Lett. **B353**, 477 (1995).

- [20] S.P.Martin, M.T.Vaughn, **hep-ph/9311340**.
- [21] B.C.Allanach, S.F.King, *Phys.Lett.* **B328**, 360 (1994).
- [22] S.G.Gorshny, A.L.Kataev, S.A.Larin, *Phys.Lett.* **B135**, 457 (1984).
O.V.Tarasov, A.A.Vladimirov, A.Y.Zharkov, *Phys.Lett.* **B93**, 429 (1980).
- [23] R.Barbieri, L.J.Hall, A.Strumia, *Nucl.Phys.* **B445**, 219 (1995).
- [24] Particle Data Book, *Phys.Rev.* **D54**, 58 (1996)
- [25] ALEPH Collaboration (R. Barate *et al.*), Report No. CERN--PPE--97--128
(hep--ex/9710012), Sep. 1997, submitted to *Z. Phys. C*.
- [26] DELPHI Collaboration (P. Abreu *et al.*), *Eur. Phys. J.* **C1**, 1 (1998).
- [27] L3 Collaboration (M. Acciarri *et al.*), Report No. CERN--PPE--97--130,
Sep. 1997, submitted to *Phys. Lett. B*.
- [28] OPAL Collaboration (K. Ackerstaff *et al.*), Report No. CERN--PPE--97--083,
(hep--ex/9708018), submitted to *Z. Phys. C*.